Solid Earth

EGU

Late Cretaceous to Paleogene exhumation in central Europe – localized inversion vs. large-scale domal uplift

Hilmar von Eynatten[1], Jonas Kley[2], István Dunkl[1], Veit-Enno Hoffmann[1], and Annemarie Simon[1]

[1]University of Göttingen, Geoscience Center, Department of Sedimentology and Environmental Geology, Goldschmidtstrasse 3, 37077 Göttingen, Germany
[2]University of Göttingen, Geoscience Center, Department of Structural Geology and Geodynamics, Goldschmidtstrasse 3, 37077 Göttingen, Germany

**Correspondence:** Hilmar von Eynatten (heynatt@gwdg.de)

Abstract. Large parts of central Europe experienced exhumation in Late Cretaceous to Paleogene time. Previous studies mainly focused on thrusted basement uplifts to unravel the magnitude, processes and timing of exhumation. This study provides, for the first time, a comprehensive thermochronological dataset from mostly Permo-Triassic strata exposed adjacent to and between the basement uplifts in central Germany, comprising an area of at least some 250–300 km across. Results of apatite fission-track and (U–Th) / He analyses on > 100 new samples reveal that (i) kilometre-scale exhumation affected the entire region, (ii) thrusting of basement blocks like the Harz Mountains and the Thuringian Forest focused in the Late Cretaceous (about 90–70 Ma), while superimposed domal uplift of central Germany is slightly younger (about 75–55 Ma), and (iii) large parts of the domal uplift experienced removal of 3 to 4 km of Mesozoic strata. Using spatial extent, magnitude and timing as constraints suggests that thrusting and crustal thickening alone can account for no more than half of the domal uplift. Most likely, dynamic topography caused by upwelling asthenosphere significantly contributed to the observed pattern of exhumation in central Germany.

1 Introduction

Widespread intraplate compressional stresses affected central Europe in Cretaceous to Paleogene time and generated numerous basement uplifts and inverted sedimentary basins (e.g. Ziegler et al., 1995; Kley and Voigt, 2008). The base-

ment uplifts cover a large area of at least 1300 km west to east and 600 km north to south in extension. It stretches from the Ardennes in Belgium (western Rhenish Massif) to southeastern Poland (Holy Cross Mountains) and includes prominent fault-bounded blocks composed of crystalline basement rocks and pre-Permian metasedimentary rocks such as the Bohemian Massif, the Vosges and Black Forest, and the Harz Mountains (Fig. 1a). The major phase of exhumation and uplift is mostly assigned to the Late Cretaceous (Kley and Voigt, 2008). However, earlier onset of exhumation and uplift and/or its continuation into the Paleogene are proposed for certain areas and structures (e.g. Barbarand et al., 2018; Sobczyk et al., 2020).

Inverted sedimentary basins (i.e. basins that have been exhumed along former extensional faults; Cooper et al., 1989) occur partly between and within these blocks and are common further north in the Central European Basin system (see Littke et al., 2008), which includes large parts of Poland, northern Germany, the Netherlands, Denmark and the North Sea. The timing of basin inversion has been mostly assigned to Late Cretaceous to Paleogene time (e.g. Kockel, 2003; Krzywiec, 2006). Some authors have attributed all documented Mesozoic and Cenozoic uplift events in central Europe to increased tangential stress and inversion, regardless of their magnitude and extent (e.g. Ziegler et al., 1995; Sissingh, 2006). Others pointed out marked differences in the expression of these events and suggested that alternative mechanisms may be involved such as increased or decreased amplitudes of lithospheric folds due to stress buildup, stress re-
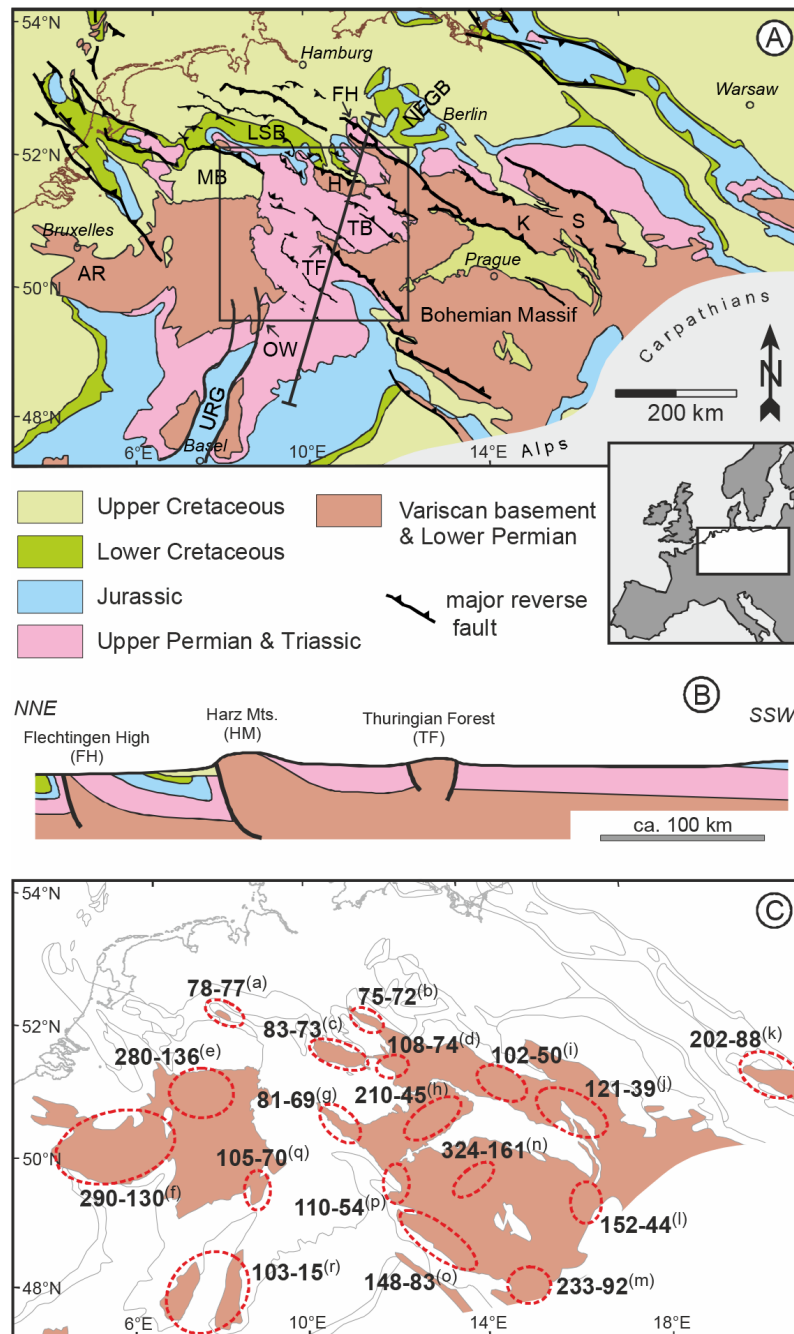
Figure 1. (a) Pre-Tertiary geological sketch map of central Europe (modified after Ziegler, 1990). The black rectangle indicates the position of the detailed geological map in Fig. 3, and the straight line indicates the trace of the section shown in **(b)**. The inset indicates the location within Europe. AR – Ardennes, FH – Flechtingen High, H – Harz Mountains, K – Karkonosze, NEGB – Northeast German Basin, LSB – Lower Saxony Basin, MB – Münsterland Basin, OW – Odenwald, S – Sudetes, TB – Thuringian Basin, TF – Thuringian Forest, URG – Upper Rhine Graben. **(b)** Simplified geological section across the central part of the study area, highlighting the major fault-bordered basement highs. For a detailed section see Fig. 4. **(c)** Compilation of apatite fission-track ages obtained on structural highs exposing Paleozoic rocks in central Europe. a: Ibbenbüren High, Senglaub et al. (2005); b: Flechtingen High, Fischer et al. (2012); c: Harz Mountains, von Eynatten et al. (2019); d: Halle volcanic complex, Jacobs and Breitkreuz (2003); e: Northern Rhenish Massif, Karg et al. (2005); f: Ardennes/Venn, Glasmacher et al. (1998), Xu et al. (2009) and references therein, Barbarand et al. (2018); g: Thuringian Forest, Thomson and Zeh (2000); h: Erzgebirge, Ventura and Lisker (2003), Lange et al. (2008), Wolff et al. (2015); i: Lusatian Block, Lange et al. (2008), Ventura et al. (2009); j: NE Bohemian Massif, Danišík et al. (2010, 2012), Migoń and Danišík (2012), Sobczyk et al. (2015, 2020); k: Holy Cross Mountains, Botor et al. (2018); l: E Bohemian Massif, Botor et al. (2017); m: S Bohemian Massif, Hejl et al. (2003); n: Barrandian, central Bohemian Massif, Glasmacher et al. (2002); o: Bavarian Forest, Vamvaka et al. (2014); p: W Bohemian Massif, Hejl et al. (1997); q: Odenwald, Wagner (1968); r: Black Forest/Vosges, Timar-Geng et al. (2006), Link (2009), Dresmann et al. (2010), Meyer et al. (2010).

laxation relaxation or dynamic topography (Nielsen et al., 2005; Deckers and van der Voet, 2018; Kley, 2018).

This paper aims at a comprehensive understanding of the Cretaceous to Paleogene exhumation in central Europe from a thermochronological point of view. We (i) review the existing thermochronological data on cooling and exhumation in central Europe, (ii) present new thermochronological data from the main study area in the central part of central Europe, (iii) integrate apatite fission-track (AFT) and (U–Th) / He (AHe) data through thermal modelling that allows for estimating the thickness of eroded sequences, and (iv) discuss various models to explain the temporal and spatial pattern of exhumation and uplift in central Europe.

2 Geological setting

Central Europe has been an intraplate region since the Variscan orogeny that terminated about 300 Myr ago (e.g. Ziegler, 1987; Oncken, 1997). Its post-orogenic history began with the evolution and demise of the "Rotliegend" wide rift in Permian time (Lorenz and Nicholls, 1976). From the latest Permian through the Mesozoic a continuous cover of sediments was deposited over large parts of central Europe. These sediments belong to the intracontinental Southern Permian Basin in the north (Littke et al., 2008; Doornenbal and Stevenson, 2010) and to the proximal Tethys shelf in the south. Both basins were connected via an intervening platform and at times formed a contiguous region of marine deposition, e.g. in Middle Triassic (Muschelkalk) and Early Jurassic time (Ziegler, 1990). The long-lasting slow subsidence in this system of basins was mostly of thermal origin (Cacace and Scheck-Wenderoth, 2016). Nevertheless, distributed and intermittent extension of generally low magnitude affected varying areas from the latest Permian to the Early Cretaceous (Geluk, 1999; Mohr et al., 2005; Warsitzka et al., 2019). Despite the evidence for some large extensional faults (Best, 1996; Baldschuhn and Kockel, 1999; De Jager, 2003), normal fault offsets typically do not exceed a few hundred metres and there is no associated volcanism. Periods of intensified extension are recognized in Late Triassic time and, for our area, in the Late Jurassic to Early Cretaceous when the Lower Saxony Basin formed (Ziegler, 1990; Stollhofen et al., 2008). Extension was centred on a belt stretching from the southern North Sea over the Netherlands and northern Germany to Poland. The southern border of this belt is sometimes abrupt and sometimes gradual, involving normal faults at considerable distance from the main preserved depocentres (Kley et al., 2008; Danišík et al., 2012). Very subtle Mesozoic extension structures occur on the Helvetic shelf in the southwest (Wetzel et al., 2003; Malz et al., 2015).

The tectonic regime changed fundamentally from extension to contraction in Late Cretaceous time (Ziegler, 1987). Syntectonic basins formed along the margins of inverting sub-basins and uplifting basement blocks (Voigt, 1963; Krzy-

wiec, 2002; Voigt et al., 2004; von Eynatten et al., 2008). The area of contraction closely coincides with the previous extension tectonics, even though not all major thrust faults are reactivated normal faults (Voigt et al., 2009). South of the main inversion axis extending from the North Sea basins to the Polish Trough, contraction attenuates abruptly or gradually. For instance, shortening structures of small magnitude are widespread in the German uplands. Mesozoic structures in the Southern Permian Basin and the northern Alpine Molasse basin are sealed by an extensive cover of locally latest Cretaceous but mostly Cenozoic sediments (Bachmann et al., 1987; Baldschuhn et al., 2001; Krzywiec and Stachowska, 2016; Voigt et al., 2021).

In Germany, uplift and erosion in Mesozoic and/or Cenozoic time are evidenced by large areas where the Variscan basement and Permian to Triassic strata are exposed today. The Rhenish and Bohemian massifs are commonly interpreted as long-lived highs that never had a substantial cover of Permo-Mesozoic sediments (Ziegler, 1990), although this model has been recently challenged for parts of the Rhenish Massif (Augustsson et al., 2018). Between these massifs, Triassic strata were continuous from northern to southern Germany (Fig. 1a). For Jurassic and Cretaceous time much of the sedimentary record, if any, has been lost due to erosion in the central part of Germany (Fig. 1b). Remnants of Cenozoic strata show that denudation to the level of Triassic strata was completed by Paleogene or Neogene time, varying by region (Bundesanstalt für Geowissenschaften und Rohstoffe, 1993).

Several processes have been proposed to have driven Late Cretaceous to Paleogene exhumation in central and western Europe. There is a consensus that Late Cretaceous inversion (often termed the "Subhercynian" event) was caused by far-field tectonic stresses related by different authors either to Alpine collision (e.g. Ziegler, 1987; Stackebrandt and Franzke, 1989; Ziegler et al., 1995; Krzywiec, 2006) or the onset of Africa–Iberia–Europe convergence (Kley and Voigt, 2008). In contrast, the Paleogene ("Laramide" and "Pyrenean") uplift events have received very different interpretations. Many authors attributed them to continued, if weaker, shortening and inversion (Ziegler, 1990; De Jager, 2003; Sissingh, 2006; Holford et al., 2009b) or long-wavelength folding (Deckers and van der Voet, 2018). Nielsen et al. (2005) argued instead that the Laramide event reflects stress relaxation. This concept is consistent with numerical modelling suggesting that plate coupling across the Iberia–Europe boundary rapidly decreased with increasing incorporation of mechanically weak continental crust (Dielforder et al., 2019), but it does not correctly predict the pattern of Laramide uplift and subsidence in some basins (Deckers and van der Voet, 2018). Paleogene regional exhumation of the Irish Sea has been explained as an isostatic response to magmatic underplating (Brodie and White, 1994; Ware and Turner, 2002). Kley (2018), based on its very large areal extent, advocated dynamic topography and lithospheric thinning (see also Meier et al., 2016) as the causes of

Laramide uplift. In this paper we focus on the timing, magnitude and possible mechanisms of Late Cretaceous and Paleogene exhumation in Germany. Because of the coincidences in time with widespread exhumation events all over central Europe, these will be reviewed in the next section.

3 Review of thermochronological data

The available thermochronological data on Mesozoic to Tertiary exhumation in central Europe are widespread and focus on individual regions exposing Paleozoic basement rocks. Only near-surface samples (except for a few drill cores with a sampling depth < 500 m) are considered for this compilation to ensure comparability. The most comprehensive dataset is available for apatite fission-track data, which are summarized in Fig. 1c with respect to individual regions and the respective range of AFT ages. Many regions show a predominance of Cretaceous AFT ages; however, others show a much broader range including Jurassic and Permo-Triassic ages and/or a noticeable contribution of Tertiary ages.

The Ardennes, forming a large part of the western Rhenish Massif in the Rhenohercynian zone of the central European Variscan orogeny (location f in Fig. 1c), are predominantly composed of very low-grade Devonian to Carboniferous metasedimentary rocks, with some early Paleozoic low- to medium-grade inliers. Low-T thermochronology comprises mostly AFT data along with some zircon fission-track (ZFT) data. The latter indicate ages between 422 and 218 Ma, while AFT ages range from Permian to Early Cretaceous (290 to 130 Ma; Glasmacher et al., 1998; Xu et al., 2009, and references therein; Barbarand et al., 2018). Although the age range is rather consistent across the various studies, interpretations based on thermal modelling and various geological evidence are quite different. Xu et al. (2009) propose slow exhumation and cooling for most of the Mesozoic, followed by accelerated cooling since middle Eocene time. Glasmacher et al. (1998) suggest a major phase of cooling in the middle Cretaceous (120 to 80 Ma) along with approximately 2000 m of exhumation. In contrast, Barbarand et al. (2018) use paleoweathering geochronology based on Mn-oxide phases to constrain the thermochronological modelling. They suggest Late Jurassic to Early Cretaceous uplift and erosion of the Ardennes Massif, which subsequently stayed close to the surface until the present. For the northeastern Rhenish Massif, on the right side of the River Rhine, Karg et al. (2005) reported AFT ages ranging from 291 to 136 Ma (location e in Fig. 1c). The data indicate cooling in the late stages and/or after the Variscan orogeny. Triassic to Jurassic sedimentation is interpreted below 1000 m in thickness, and the samples remained in the apatite partial annealing zone (PAZ) during most of the Mesozoic. Final uplift and denudation did not start before the Late Cretaceous, with slightly accelerated cooling in the Tertiary (Karg et al., 2005). Similar data have already been reported by

Büker (1996) for the same area (AFT 286–159 Ma). No thermochronological data have been published so far from the eastern margin of the Rhenish Massif; however, some new data will be presented in this study.

East to northeast of the Rhenish Massif, several thrusted basement blocks expose Paleozoic crystalline and/or metasedimentary rocks at the surface. These are the Ibbenbüren High, the Flechtingen High, the Harz Mountains and the Thuringian Forest (a, b, c and g in Fig. 1c, respectively). They are all characterized by long apatite fission tracks and narrow track length distributions, and despite the wide area and a pretty high number of samples ($n = 41$) the AFT age range is impressively tight, i.e. fully restricted to Campanian time (83–72 Ma; Thomson and Zeh, 2000; Senglaub et al., 2005; Fischer et al., 2012; von Eynatten et al., 2019). For the Harz Mountains, the observation of rapid Late Cretaceous exhumation is further supported by zircon (U–Th) / He (ZHe) and AHe thermochronology (von Eynatten et al., 2019) as well as independent evidence from facies distribution and provenance information from well-dated syntectonic sediments in the foreland (Voigt et al., 2006; von Eynatten et al., 2008). ZFT data from the four basement blocks range from the latest Carboniferous (306 Ma) to latest Triassic (202 Ma). While the oldest ages may directly reflect cooling after the Variscan orogeny, most ages are Permo-Triassic and interpreted as mixed ages, reflecting partial reset due to widespread Permo-Mesozoic burial heating (Fischer et al., 2012; von Eynatten et al., 2019). Slightly east of the Harz Mountains, the Halle volcanic complex (location d in Fig. 1c) consists of Permo-Carboniferous felsic volcanic rocks yielding thermochronological data rather similar to the Harz Mountains, although AFT ages are slightly older (ZFT 231–194 and AFT 108–74 Ma; Jacobs and Breitkreuz, 2003).

The Bohemian Massif represents the largest inlier of basement rocks exposed in central Europe (Linnemann et al., 2008). It is mainly composed of late Neoproterozoic to early Paleozoic (Cadomian) and late Paleozoic (Variscan) granitoids with a large variety of metamorphic rocks comprising late Neoproterozoic to Carboniferous protoliths and metamorphic grades from very low grade to high grade, including ultrahigh-pressure metamorphism (Kroner et al., 2008; Schönig et al., 2020). Morphologically, the Bohemian Massif comprises several mountain ranges. Their low-temperature evolution has been investigated by numerous studies (as reviewed below) in order to unravel the post-Variscan exhumation and uplift history of the Bohemian Massif. Results indicate a complex spatial pattern caused by various partly superimposed processes including Mesozoic burial, Late Cretaceous exhumation due to far-field compression and/or reheating, and exhumation related to the European Cenozoic Rift System and associated volcanism (e.g. Danišík et al., 2012).

The northern margin of the Bohemian Massif can be roughly separated, from west to east, into the Erzgebirge, the Lusatian Block and the Sudetes including the Karkonosze Mountains. The central Erzgebirge is character-

ized by medium- to high-grade metamorphic rocks, including relics of ultrahigh-pressure metamorphism, surrounded by lower-grade metasedimentary rocks and intruded by late Variscan granitoids. AFT data reveal a large age spread from 210 to 45 Ma with predominantly (19 out of 24) Late Jurassic and Cretaceous ages (location h in Figs. 1c and 2a; Lange et al., 2008). Similar ages are reported from a borehole in the western Erzgebirge (Ventura and Lisker, 2003). The diverse spatial pattern of thermochronological data is supported by ZHe and AHe data and indicates dissection into individual structural blocks, variable Mesozoic burial and hydrothermal activity, significant Late Cretaceous exhumation, and only minor Cenozoic overprint (Wolff et al., 2015). The Lusatian Block (location i in Fig. 1c), which is separated from the Erzgebirge by the Elbe fault zone, is characterized by mostly Late Cretaceous AFT ages, as reported by two different studies. The first is based on 28 predominantly granodiorite samples covering the entire area, which yield an AFT age range of 102 to 50 Ma (Fig. 2a; Lange et al., 2008). The second is based on 10 samples from three boreholes (sample depth < 500 m) from the northern and southern boundaries of the block, which yield a tighter Late Cretaceous AFT age range from 94 to 72 Ma (Ventura et al., 2009). Roughly similar data are reported from various studies of the Sudetes, forming the structurally complex NE margin of the Bohemian Massif (location j in Fig. 1c). The Variscan granite intrusion of the Karkonosze Mountains experienced punctuated Late Cretaceous fast cooling and exhumation as evidenced by ZHe (98 Ma), AFT (90–82 Ma) and AHe (87–79 Ma) thermochronology (Danišík et al., 2010). Metamorphic rocks to the north of the intrusion show a somewhat broader Cretaceous age range (121–63 Ma; Martínek et al., 2006, 2008; cited in Migoń and Danišík, 2012). From the easternmost part of the intrusion and adjacent metamorphic rocks, Early Cretaceous ZHe ages (131–100 Ma) and Cretaceous to Paleogene AFT ages (106–51 Ma) are reported (Sobczyk et al., 2015). In the SE Sudetes, crystalline rocks of the Rychlebské hory Mountains region reveal Late Cretaceous to Paleocene exhumation history evidenced by ZHe (79 and 89 Ma) and AHe (90–69 Ma) data along with slightly younger AFT ages (81–39 Ma); the youngest of them were most likely influenced by Cenozoic volcanism (Danišík et al., 2012). However, nearby samples from small crystalline massifs reveal similar Late Cretaceous to Eocene AFT ages (84–45 Ma), which are interpreted to reflect Late Cretaceous onset of cooling with a climax in the Paleocene to middle Eocene (Sobczyk et al., 2020). The cumulative distribution of all AFT ages from the NE margin of the Bohemian Massif shows distinct age groups in the Late Cretaceous, around the $K–T$ boundary and in the Paleocene to Eocene (Fig. 2a).

At the eastern margin of the Bohemian Massif, the Moravo–Silesian zone exposes lower Carboniferous synorogenic clastic sedimentary rocks (Moravo–Silesian Culm Basin, location l in Fig. 1c), which experienced post-Variscan anchimetamorphic overprint. ZHe ages range from 303–163 Ma, while AFT ages range from Late Jurassic (152 Ma) to Eocene (44 Ma), with the majority of ages belonging to the Late Cretaceous (Fig. 2b; Botor et al., 2017). In the southernmost part of the Bohemian Massif (Waldviertel) AFT ages from granitoids and gneisses show a broad range from 233–92 Ma (location m in Fig. 1c; Hejl et al., 2003). Despite some spatial variation and generally older ages towards the northeast, thermal modelling suggests general Jurassic to Early Cretaceous cooling, followed by some reburial in the Late Cretaceous. Cenozoic bulk denudation is estimated of the order of 1–3 km (Hejl et al., 2003). At the southwestern margin of the Bohemian Massif, the crystalline rocks of the Bavarian Forest (location o in Fig. 1c) yield AFT ages that are almost entirely Cretaceous (148–83 Ma), with most of them falling into the Late Cretaceous (Fig. 2c; Vamvaka et al., 2014). Thermal modelling of these data suggests enhanced heat flow in the Middle Jurassic to Early Cretaceous, likely caused by lithospheric extension, followed by Late Cretaceous to Paleogene cooling (Vamvaka et al., 2014). At the western margin of the Bohemian Massif (Oberpfalz; location p in Fig. 1c), Permo-Triassic ZFT ages (283–215 Ma) are thought to indicate post-Variscan unroofing and denudation (Hejl et al., 1997). This observation is complemented by a series of AFT data that reveal a relatively tight age cluster (110–54 Ma), implying accelerated denudation in Late Cretaceous to Paleogene time (Fig. 2c).

In contrast to the numerous studies from the margins of the Bohemian Massif reporting Cretaceous AFT median ages (Fig. 2a–c), data from the Tepla–Barrandian and adjacent areas in the centre of the Bohemian Massif are relatively scarce and indicate remarkably older AFT ages (324–161 Ma, location n in Fig. 1c). They are interpreted to indicate late Variscan cooling, reburial during the post-Variscan Molasse stage and relatively slow Mesozoic cooling (Glasmacher et al., 2002; Suchý et al., 2019).

Northeast of the Bohemian Massif, the Holy Cross Mountains in SE Poland (location k in Fig. 1c) expose Paleozoic sedimentary rocks that experienced deformation during the Variscan orogeny, followed by significant burial during prolonged Permo-Mesozoic subsidence within the Mid-Polish Trough of the Polish Basin and exhumation in the Late Cretaceous to Paleocene (e.g. Krzywiec et al., 2009). The available thermochronological data reveal mostly late Paleozoic ZHe ages (417–283 Ma) that are generally younger than the sedimentation ages, along with a few scattered Mesozoic AFT ages (202–88 Ma) and Late Cretaceous to Paleogene AHe ages (91–43 Ma). Thermal modelling indicates late to post-Variscan (Carboniferous to Permian) cooling from at most deep diagenetic temperatures that were reached during the Variscan orogeny. Mesozoic burial and Late Cretaceous fast cooling and exhumation are most pronounced in the eastern part of the Holy Cross Mountains (Botor et al., 2018).

The Upper Rhine Graben (URG) forms part of the Cenozoic European Rift System and exposes crystalline basement domains at its exhumed flanks. The most prominent ones
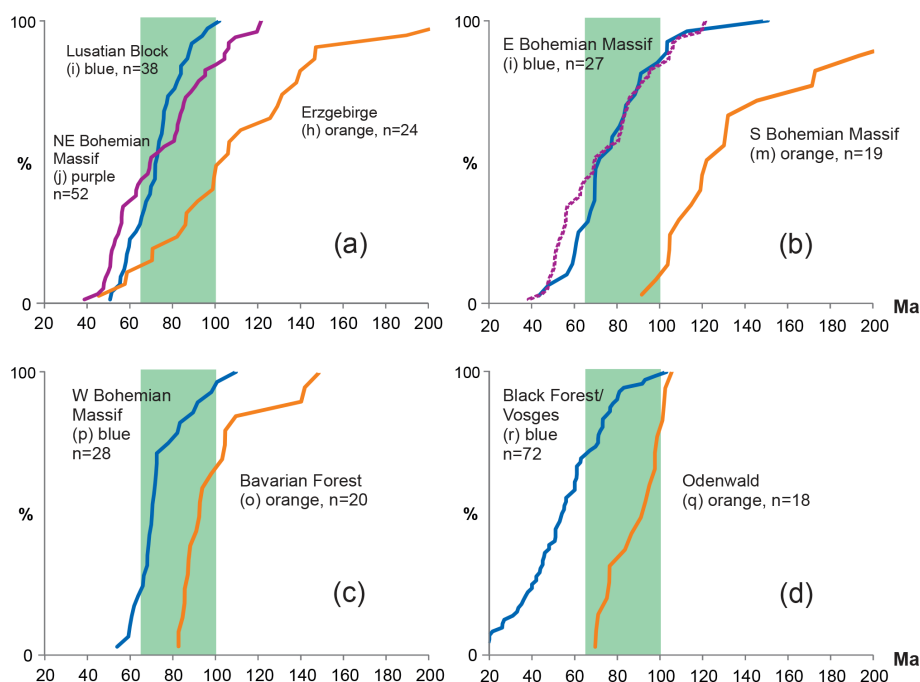
Figure 2. Cumulative frequency distributions of apatite fission-track data from various regions across central Europe. Characters in brackets refer to locations in Fig. 1; for references see the caption to Fig. 1. The stippled purple line in **(b)** is from the NE Bohemian Massif, like in **(a)**, for reference. The green area indicates the time interval of the Late Cretaceous.

are located adjacent to the southern URG, i.e. the Vosges at the western and the Black Forest at the eastern flank (location r in Fig. 1c). Thermochronological data show broad age ranges, reflecting the complex superposition of variable Mesozoic hydrothermal activity (that reached the zircon partial annealing zone, most likely in Jurassic time), Late Cretaceous cooling and exhumation, and Cenozoic reheating related to rifting in the URG followed by final exhumation (Timar-Geng et al., 2006; Link, 2009; Dresmann et al., 2010; Walter et al., 2018). ZFT ages range from the Late Carboniferous to Early Cretaceous (312–109 Ma; the youngest ages are related to a fault zone at the southern margin of the Black Forest; Dresmann et al., 2010), while AFT ages range from the Cretaceous to Miocene (103–15 Ma) with distinct age components in the Late Cretaceous and Paleogene (Fig. 2d). AHe data yield only Cenozoic ages ranging from the Paleocene to early Miocene (61–20 Ma; Link, 2009). Adjacent to the northern URG, the Odenwald region (location q in Fig. 1c) exposes Variscan granitoids from the Mid-German Crystalline Rise, which yield a relatively tight Cretaceous AFT age range (105–70 Ma, Fig. 2d; Wagner, 1968). Late Cretaceous AFT ages (∼ 80–70 Ma) of the Odenwald and the opposing western flank of the URG (Palatinate Forest) are confirmed by Link (2009). The almost entire restriction to Late Cretaceous AFT ages point to an essentially similar thermal evolution, as described before for the Thuringian Forest and the Harz Mountains further northeast (Fig. 1).

In summary, thermochronological data from most of the basement uplifts in central Europe provide evidence for a phase of Late Cretaceous cooling and exhumation. This is most obvious and accentuated for an approximately 300×250 km region in central Germany, encompassing the Harz Mountains and the Thuringian Forest, as well as the Flechtingen and Ibbenbüren High in the north and the Odenwald in the south (i.e. the main study area as outlined in Sect. 4). Further south, at the flanks of the URG, this event also seems important but is partly masked by Cenozoic rifting and magmatic–hydrothermal activity. Towards the east, the margins of the Bohemian Massif provide ample evidence for Late Cretaceous cooling and exhumation, with variable expansion into the Paleogene, especially at its western and eastern margins. Even for the most distant areas in the west (Ardennes) and east (Holy Cross Mts.), Late Cretaceous to Paleogene cooling is considered a relevant part of the post-Variscan evolution.

4   Study area in central Germany and sample coverage

The main study area approximately coincides with the northern half of the German uplands region ("Mittelgebirge", Fig. 3). It is underlain by a mostly sedimentary substrate of variable lithology and structural complexity. Its northern part borders the inverted Lower Saxony Basin (LSB) in the west and the Northeast German Basin (NEGB) in the east (Fig. 1). The southern border of the LSB is thrust onto the

Cretaceous Münsterland Basin along the Osning Fault, a regional reactivated normal fault. The Münsterland Basin overlies the margin of the Rhenish Massif. The NEGB is bounded to the south by the Gardelegen reverse fault, which creates a major basement step (Fig. 4). Two additional prominent basement uplifts related to major Cretaceous thrust faults follow towards the south (Harz Mountains and Thuringian Forest), separated by wide synclinal areas dominated by Triassic strata. The Gardelegen Fault and northern Harz thrust fault are associated with syn-inversion Cretaceous growth strata in the Northeast German Basin and the Subhercynian Basin, respectively. The Thuringian Forest passes into the Thuringian Schiefergebirge and the Bohemian Massif towards the southeast. All three are bordered by the Franconian Line, a regional southwest-directed reverse fault. The Osning Fault and Franconian Line approximately mark the southwestern limit of strong Mesozoic deformation. They are connected by an array of smaller fault zones (e.g. the Hessian grabens), most of which are extensional structures displaying signs of inversion (e.g. Lotze, 1948; Kley et al., 2008). Similar fault zones south of the Franconian Line are the southernmost expression of Late Cretaceous inversion on the transect in Fig. 4 (Kämmlein et al., 2020). The Odenwald and Spessart in the west are uplifts of the Variscan basement not associated with major Cretaceous thrust faults (Fig. 3). The gently warped Franconian platform underlies the cuesta landscape of southern Germany ("Süddeutsches Schichtstufenland") and dips under the Cenozoic of the northern Alpine Molasse foreland basin in the south.

A total of 10 major geological–structural units are defined in the study area considering the major fault patterns as well as contrasts in the thickness, facies and preservation of the Mesozoic–Cenozoic sequences (Fig. 5). Only the Lower Saxony Basin and the Harz Foreland Basin show a more or less complete record of Mesozoic sedimentation. In the central part of the study area, drained by the Werra, Fulda and Weser rivers (WFW), as well as the Thuringian Basin and the Franconian platform, Triassic sedimentary rocks are exposed at the surface, while Jurassic and Cretaceous strata are rarely preserved (Fig. 3). The latter also applies for the Leipzig Basin, but a largely continuous Tertiary cover is preserved there. The deepest denudation has obviously affected the crystalline basement highs, namely the Harz Mountains, Thuringian Forest, Rhenish Massif and Bohemian Massif, where Variscan metamorphic and intrusive rocks as well as some Permian deposits are exposed at the surface, and no stratigraphic evidence is available for the thickness of the former Mesozoic and Cenozoic cover.

Samples

More than 300 samples have been collected, and the results are based on the analysis of more than 100 samples suitable for thermochronology, covering an area of about 300 km in E–W extension and 220 km in N–S extension (see Supple-
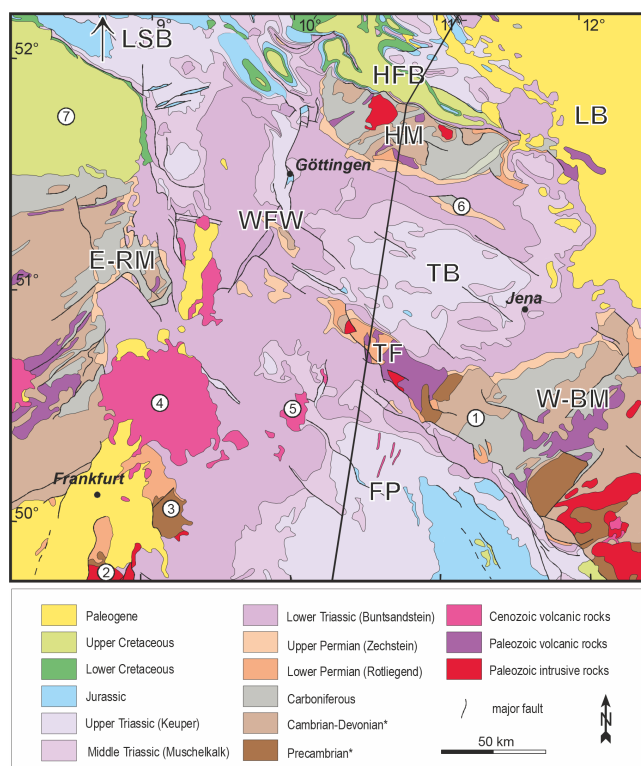
Figure 3. Geological map of the study area (simplified after Bundesanstalt für Geowissenschaften und Rohstoffe, 2004; * affected by a variable degree of metamorphic overprint). Abbreviations are used for geological–structural units mentioned in the text and correspond to the stratigraphical columns in Fig. 5a: LSB – Lower Saxony Basin, HFB – Harz Foreland Basin, HM – Harz Mountains, LB – Leipzig Basin, TB – Thuringian Basin, TF – Thuringian Forest, WFW – Werra–Fulda–Weser region, E-RM – eastern Rhenish Massif, FP – Franconian platform, W-BM – western Bohemian Massif. Locations of further geographical–geological units mentioned in the text are labelled with numbers: (1) Thuringian Schiefergebirge, (2) Odenwald, (3) Spessart, (4) Vogelsberg, (5) Rhön, (6) Kyffhäuser High, (7) Münsterland Basin. The black line indicates the trace of the section shown in Fig. 4.

ment S1 and S2). Because the basement uplifts are largely well characterized in terms of thermochronology (Sect. 3), the sampling strategy focuses on areas between these uplifts such as the Thuringian Basin, the Weser hills (Weserbergland) and the Hessian grabens as well as areas marginal to the Rhenish Massif and the western Bohemian Massif. Moreover, a couple of samples have been taken from the Thuringian Forest and the Franconian platform to trace the thermal history of the Triassic strata towards the south.

Samples comprise mostly siliciclastic rocks from the Early Triassic (Buntsandstein, $n = 63$), late Paleozoic (Devonian to Permian, $n = 33$), Late Triassic (Keuper, $n = 8$) and Early Jurassic ($n = 1$). Further samples include Variscan granite ($n = 2$ including one granite pebble from Permian clastics), Devonian diabase ($n = 2$) and Permian rhyolite ($n = 1$). The
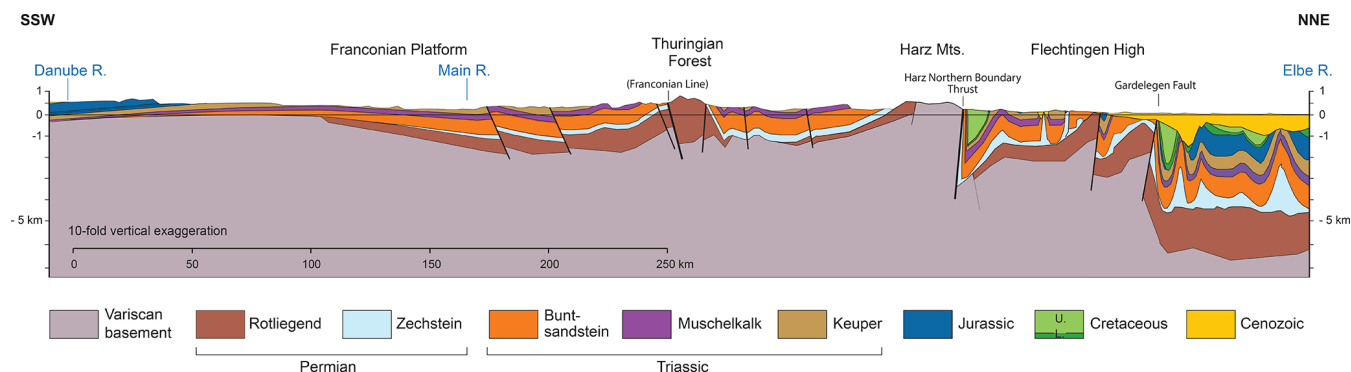
Figure 4. Regional cross section from the Danube to the Elbe (location in Fig. 3). Strong inversion-related deformation from the Thuringian Forest towards the north contrasts with long-wavelength undulations of the area to the south. Faults are shown schematically but with correct general dip. The area north of the Harz Mountains is simplified from Jähne (in Kley et al., 2008, p. 105) and Malz et al. (2020).

distribution of the samples with respect to stratigraphical levels of the different geological–structural units in the study area is outlined in Fig. 5a. Almost all samples are surface samples except for four drill-core samples taken from depths shallower than 500 m. All 110 samples listed were used for apatite fission-track analysis, while 37 of them were also suited for apatite (U–Th) / He thermochronology.

## 5   New thermochronological data

5.1   Methods

For apatite fission-track analysis, the external detector method was used (Gleadow, 1981). Highly enriched apatite concentrates were embedded in epoxy resin, diamond-polished in five steps and etched by 5.5 N HNO_3 solution for 20 s at 21 °C (Donelick et al., 1999). The apatite grain mounts with the etched spontaneous tracks were covered with freshly cleaved muscovite sheets as external track detectors and irradiated with thermal neutrons in the research reactor of the TU Munich in Garching. A Corning glass dosimeter (CN5) was used to monitor the neutron fluence. After irradiation the tracks in the external detectors were revealed by etching in 40 % HF for 40 min at 21 °C. Spontaneous and induced fission tracks were counted under 1000× magnification using a Zeiss Axioskop microscope equipped with a computer-controlled stage system (Dumitru, 1993). Only apatite crystals with a well-polished surface parallel to the crystallographic c axis were considered. In most cases 20 to 25 grains were measured per sample. Additionally, the Dpar values were measured in each dated apatite crystal, and the lengths of horizontal confined tracks were determined in most of the samples. AFT ages were calculated using the zeta age calibration method (Hurford and Green, 1983) with the standards listed in Hurford (1998). Data processing and plotting were performed with the TRACKKEY software (Dunkl,

2002), while errors were calculated using the classical procedure described in Green (1981).

For apatite (U–Th) / He analysis the crystals were wrapped in platinum capsules and heated in the full-metal extraction line by an infrared laser for 2 min in high vacuum. The extracted gas was purified using a SAES Ti–Zr getter kept at 450 °C. The chemically inert noble gases and a minor amount of other rest gases were then expanded into a Hiden triple-filter quadrupole mass spectrometer equipped with a positive ion-counting detector. Beyond the detection of helium the partial pressures of some rest gases were continuously monitored (H_2, CH_4, H_2O, N_2, Ar and CO_2). He blanks were estimated using the same procedure on empty Pt tubes, and the crystals were checked for degassing of He by sequential reheating and He measurement. The amount of He extracted in the second runs is usually below 1 %. Following degassing, samples were retrieved from the gas extraction line and spiked with calibrated ^{230}Th and ^{233}U solutions. The apatite crystals were dissolved in a 4 % HNO_3 + 0.05 % HF acid mixture in Savillex Teflon vials. Each sample batch was prepared with a series of procedural blanks and spiked normals to check the purity and calibration of the reagents and spikes. Spiked solutions were analysed by a Thermo iCAP-Q ICP-MS. The ejection correction factors (Ft) were determined for the single crystals by a modified algorithm of Farley et al. (1996) using an in-house spreadsheet.

Single-crystal aliquots were dated, usually with three aliquots per sample. The crystals were inspected for inclusions under 250× magnification and cross-polarized light. Inclusion- and fissure-free, intact, mostly euhedral apatite crystals were selected from igneous samples. The siliciclastic samples, however, contain mostly well-rounded apatite grains with dull or rugged surfaces. The interiors of such grains were controlled in alcohol immersion, but due to the limited optical resolution they may contain tiny inclusions that were overlooked and may have led to minor contributions of excess helium. The shape parameters for the Ft correction were determined and archived by multiple digi-
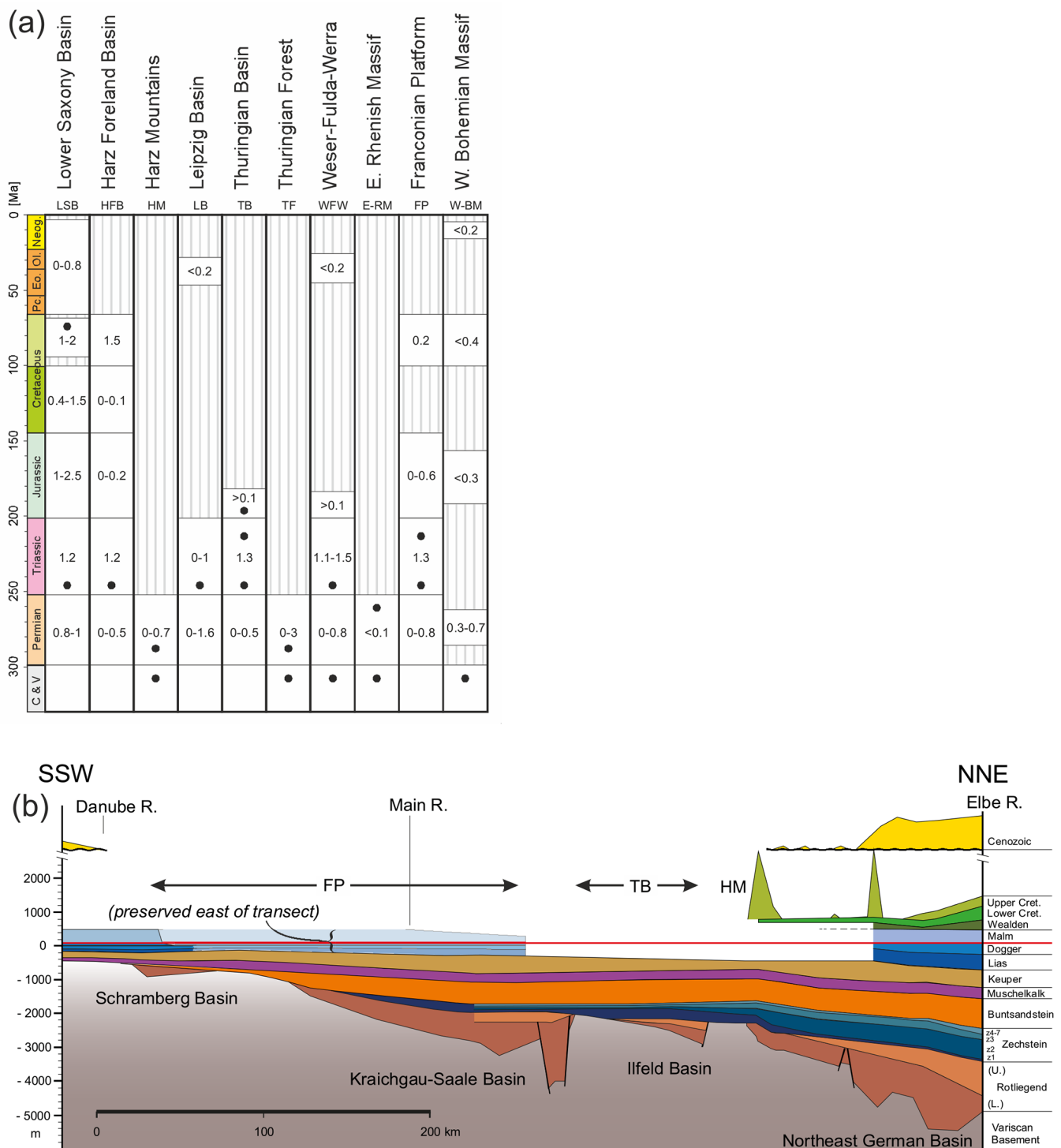
Figure 5. (a) Compilation of stratigraphical data for various geological–structural units of the study area as mentioned in the text and indicated in Fig. 3. The approximate thicknesses of the strata are given in kilometres. C and V: Carboniferous (meta)sedimentary and Variscan metamorphic or igneous basement rocks, respectively. Black dots represent the stratigraphic levels of the samples used for thermochronology. **(b)** Transect along the cross section in Fig. 4, showing primary variations in thickness and different preservation. The units shown in **(a)** are projected onto the transect if appropriate. Zechstein to Triassic strata exhibit a relatively monotonous southward thickness decrease and onlap onto Variscan basement of the southern basin margin. Eroded thicknesses of Jurassic and Cretaceous strata from the central segment are primarily constrained by thermochronological data. Thickness data are from Boigk and Schöneich (1974) and Hoth et al. (1993); contour maps can be found in Freudenberger and Schwerd (1996) and Franke (2020).

tal microphotographs. The morphology of the euhedral crystals was approximated by the combination of prismatic and pyramidal faces, while in the case of rounded grains it was approximated by oblate and prolate ellipsoids.

5.2 Results of apatite fission-track analysis

The AFT apparent ages range from 208–53 Ma, with the majority of ages ($\sim$ 60 %) falling into the Late Cretaceous (Fig. 6 and Supplement S3). Paleocene to earliest Eocene ages contribute $\sim$ 21 % and Early Cretaceous ages $\sim$ 17 % to the entire distribution, while older ages are very rare. Track length measurements reveal mean values between 11.5 and 14.1 μm and standard deviations between 0.9 and 2.7 μm (Supplement S4). Relations between track length data and apparent ages display boomerang-like shapes (Green, 1986); i.e. the youngest and the oldest ages tend to have slightly longer tracks and narrow track length distributions (Fig. 6). Dpar values range from 1.70 to 3.47 μm with a mean of 2.46 μm, pointing to overall relatively high thermal retentivity of fission tracks in the lattice of the dated apatite crystals (Donelick et al., 2005).
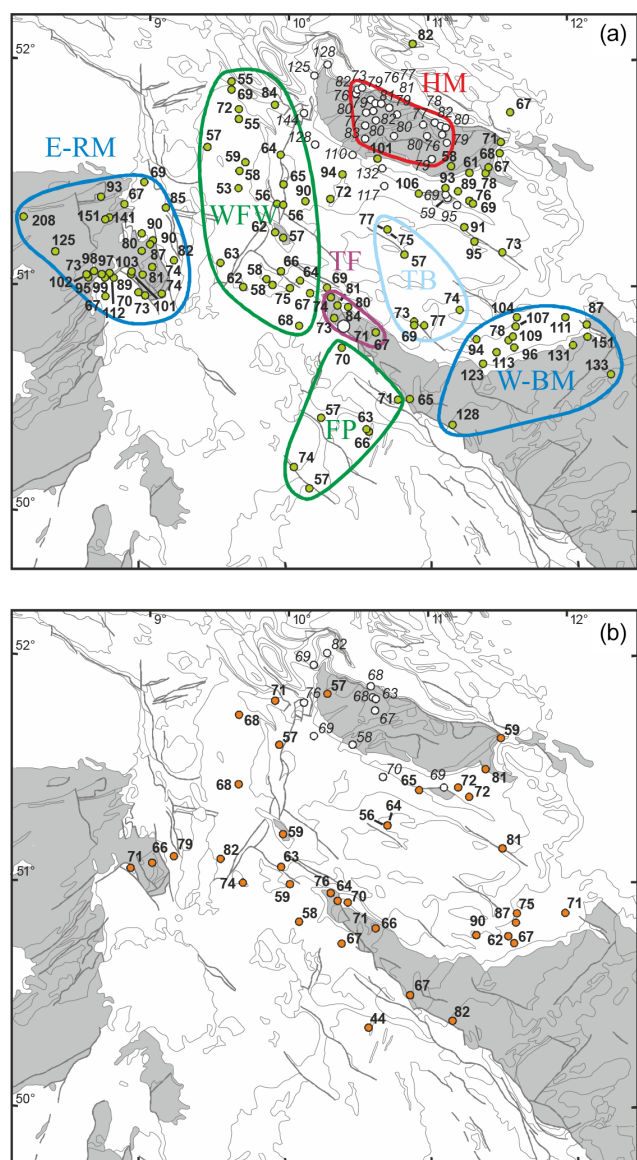
For evaluation, the new apatite fission-track data are assigned to five regions according to the spatial clustering of the samples, data coherence, and their belonging to the geological–structural units and stratigraphic levels as introduced in Figs. 3 and 4. These are the following: (i) the core of the study area formed by the Buntsandstein uplands in northern Hesse and southern Lower Saxony, drained by the Weser, Fulda and Werra rivers (WFW); (ii) Triassic of the centre of the Thuringian Basin (TB); (iii) the transition from the eastern Thuringian Basin into the Thuringian Schiefergebirge (i.e. western margin of the Bohemian Massif; W-BM); (iv) late Paleozoic to Early Triassic of the eastern margin of the Rhenish Massif (E-RM); and (v) the Franconian platform (FP) south of the Thuringian Forest (Fig. 7). The elevated basement highs of the Harz Mountains (HM) and the Thuringian Forest (TF) also yield very coherent age data. For the evaluation of these two units a few new data are combined with published data by von Eynatten et al. (2019) and Thomson and Zeh (2000), respectively. Note that not all samples are included in these seven regions.

The core region of the study area, WFW, exhibits Late Cretaceous to earliest Eocene ages (90–53 Ma). It shows a relatively large contribution of early Tertiary ages (17 out of 26) compared to the overall age distribution and includes the youngest ages of the entire study area (Fig. 7a). Remarkably, WFW includes a small basement uplift (mostly Devonian greywackes, "Werra-Grauwackensattel"), which yields a similar Paleocene AFT age as the adjacent Buntsandstein (57 vs. 62 Ma, respectively; see Fig. 7a and Supplement S1–S3). South of the Thuringian Forest and on the Franconian platform AFT data reveal a narrow Late Cretaceous to Paleocene AFT age range (74–57 Ma), rather similar to WFW. In the Thuringian Basin AFT apparent ages range from 123–
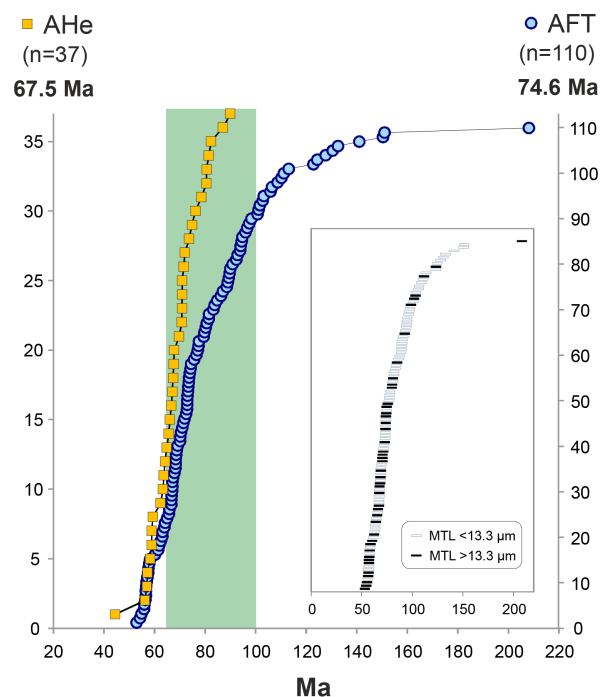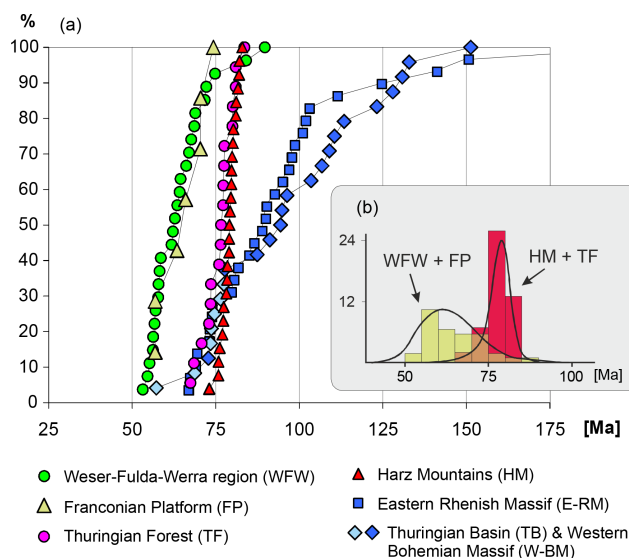

Figure 6. Cumulative frequency distributions of apatite fission-track (AFT) and apatite (U–Th) / He (AHe) ages from the study area. Bold numbers indicate the medians of the two datasets. The green area indicates the time interval of Late Cretaceous. The inset highlights the fact that long mean track lengths (MTLs) are mostly associated with AFT ages younger than $\sim$ 80 Ma.

57 Ma. Late Cretaceous ages are predominant in the central part of the basin (TB, except for one Paleocene age); however, towards its eastern margin several Early Cretaceous ages are observed (123–104 Ma). This trend towards older ages extends into the Thuringian Schiefergebirge with Early Cretaceous to Late Jurassic ages (151–131 Ma). Because this trend does not allow clear separation, the eastern Thuringian Basin and the Schiefergebirge have been grouped together (W-BM; Fig. 7a). A similar situation, although flipped in the orientation of the age trend, is observed at the eastern margin of the Rhenish Massif (E-RM). Late Paleozoic rocks within the massif reveal, besides Late Cretaceous ages, several Late Jurassic to Early Cretaceous ages (101–151 Ma) and a single Late Triassic age at the westernmost location. East of the Rhenish Massif, Lower Triassic sandstones reveal exclusively Late Cretaceous ages (90–67 Ma; Fig. 7a). The Permo-Triassic samples clustering to the southeast of the Harz Mountains and around the fault-bounded Kyffhäuser High range between 106 and 61 Ma. Due to structural complexity they were not treated as a coherent group here. The oldest age of 106 Ma occurs at the western edge of the Kyffhäuser High and suggests transition to the Early Cretaceous ages observed along the western and southern rim of the Harz (von Eynatten et al., 2019).

Figure 7. Spatial presentation of the new apatite fission-track **(a)** and (U–Th) / He ages **(b)**. The map is a simplified version of Fig. 3; grey represents Permian Rotliegend and older formations (i.e. pre-Zechstein). Coloured envelopes in **(a)** highlight the regions defined in the text and Fig. 3, where most of the samples are clustering. Small white circles in and around the Harz Mountains indicate localities of low-T thermochronology data by von Eynatten et al. (2019). The bigger white circle in the Thuringian Forest indicates the locality of the AFT samples from the Ruhla Crystalline Complex; Thomson and Zeh (2000).

Figure 8. (a) Cumulative distribution of apatite fission-track ages sorted for the individual regions outlined in Fig. 7. Note that the central Thuringian Basin data (TB) are plotted together with its eastern transition into the Bohemian Massif (W-BM) in a single cumulative curve but with a different colour. The Harz Mountains data are taken from von Eynatten et al. (2019), and the Thuringian Forest dataset is composed of our new results and data published by Thomson and Zeh (2000). **(b)** Histograms and kernel density estimates (KDEs; Vermeesch, 2012) to emphasize the highly significant contrast of Werra–Fulda–Weser (WFW) and Franconian platform (FP) data versus Harz Mountains (HM) and Thuringian Forest (TF) data, which differ by 15 to 20 Myr.

The comparison of the cumulative distributions of the individual regions reveals almost identical pairwise patterns for the following regions: (i) WFW and FP, (ii) E-RM and TB + W-BM, and (iii) the thrusted basement blocks represented by the Harz and the Thuringian Forest (Fig. 8a). The age contrast between (i) and (iii) is about 10–15 Ma, rather constant over most of the age distribution. Given the high number of samples this age contrast is highly significant (Fig. 8b). At the margins of the study area (E-RM and W-BM), the apparent ages are mostly older, including high proportions of Turonian and older ages (> 90 Ma), which tend to have a shorter track length (Fig. 6). However, their youngest Late Cretaceous age components, derived from the Lower Triassic sandstones bordering the Rhenish Massif and the central Thuringian Basin (TB), are similar to the youngest ages of the thrusted basement blocks (Fig. 8a).

5.3 Results of apatite (U–Th) / He analysis

The calculated unweighted average sample ages (referred to as AHe age) range from 90–44 Ma, with the majority of ages (∼ 62 %) falling into the Late Cretaceous (Fig. 6 and Supplement S5). The rest are Paleocene ages and a single middle Eocene age. Standard deviations of the AHe ages vary from 1 to 12 Myr. The median of all AHe ages (67.5 Ma) is younger than the median of all AFT ages (74.7 Ma; Fig. 6). The AHe cumulative age distribution overlaps the AFT distribution for the youngest ages.

The spatial distribution of the AHe ages is rather uniform, without a significant contrast between the individual

regions considered (Fig. 7b). For the core region of the study area (WFW), AHe ages range from 82 to 57 Ma, which is well in line with the overall range. In fact, the mean age of WFW is almost undistinguishable from the mean of all AHe ages (66.8 vs. 68.6 Ma, respectively). The two oldest AHe ages (87 and 90 Ma) occur in the eastern Thuringian Basin. However, a trend of increasing ages towards the Thuringian Schiefergebirge (W-BM) is not observed, in contrast to the AFT data. Similarly, no trend is visible at the eastern margin of the Rhenish Massif (E-RM). The single Eocene AHe age of 44 Ma is obtained from Late Triassic sandstone of the Franconian platform (FP) with an AFT age of 63 Ma.

6 Thermal modelling

6.1 Temperature–time paths based on low-T thermochronological data

Details of the low-T thermal history of the different regions are elucidated using the HeFTy modelling programme (Ketcham, 2005), operating with the multikinetic fission-track annealing model of Ketcham et al. (2007) and using Dpar as a kinetic parameter. For the diffusion kinetics of helium in apatite the constraints of Farley (2000) were used. For the modelling the following constraints were considered: (i) current annual mean temperature for the surface samples and the relevant borehole temperature for the drill cores, (ii) onset of the cooling history at the late stages of the Variscan orogeny at ∼ 300 Ma, (iii) surface temperature of approximately 20 °C at ca. 290–250 Ma for the Permian and 250–230 Ma for the Triassic sediments, and (iv) surface temperature of approximately 20 °C for the onset of the Paleogene burial (ca. 45–35 Ma). The latter constraint is crucial for the modelling of the study area. The Paleogene sediments are widespread and seal the erosional surface of the Permo-Triassic strata, especially in the west (E-RM) and east (Leipzig Basin, see Fig. 5a). At least the eastern part of the Thuringian Basin corresponds to a planation surface, as demonstrated by scattered remnants of thin fluvial sediments of supposedly Oligocene age ("Hochflächensedimente"; Seidel, 2003, p. 415). Thus, although these areas are currently uncovered their surface can be considered the prolongation of the Triassic–Paleogene unconformity. We allowed an unsupervised run for the modelling algorithm in the time range between the Permo-Triassic and Eocene surface temperature constraints.

The modelled temperature–time (tT) paths are rather uniform within the individual regions outlined above; Fig. 9 shows a selection covering all regions including a northern and a southern example for the core region WFW (Fig. 9d and e, respectively). A prominent feature of the tT paths obtained in many samples is a characteristic inflexion at around 90–70 Ma indicating the onset of cooling. It appears in all Triassic samples from the WFW, FP and TB regions, but also

in the basement samples of TF. If we zoom into the post-90 Ma cooling paths a striking difference can be recognized for the samples from WFW and the Franconian platform when compared to the samples from the Thuringian Forest and the Harz Mountains (see pairwise comparison of the tT paths in Fig. 9a vs. d and b vs. e). The former show a quasi-linear cooling path between the inflexion point and the age of the onlapping Paleogene sediments, while the basement highs (TF and HM) show a more hyperbolic cooling trend (i.e. initial quick cooling followed by slower cooling). This observation explains, besides the slightly younger inflexion points, the significantly younger apparent ages of the WFW and FP samples.

At the boundaries of the study area, the eastern flank of the Rhenish Massif (E-RM) and the western flank of the Bohemian Massif (W-BM), the time–temperature paths (Fig. 9g and h) are clearly different compared to both the central part and the internal basement highs: the thermal climax is older and mostly Jurassic in age, and the Late Cretaceous inflexion does not appear except for samples having approximately 80 Ma or younger AFT apparent ages (Fig. 7a). The samples selected for illustration in Fig. 9 (g and h) represent the > 90 Ma AFT ages, which are dominant in the late Paleozoic rocks detected at the margins of both massifs (W-BM and E-RM at 131 and 141 Ma, respectively).

6.2 Reconstruction of the missing sequence

The very characteristic thermal paths described above and the lithology and thickness conditions of the post-Triassic sequences in the well-preserved basins (Fig. 5) form the base for the reconstruction of the missing sequences from the deeply eroded regions, where only Variscan basement rocks and Permo-Triassic formations are exposed at the surface. The modelling was performed by a combination of PetroMod (Schlumberger) and HeFTy (Ketcham, 2005) software.

In the first step, the stratigraphic information from the preserved surrounding basins is crucial for the modelling. The Triassic sequences have relatively constant thickness (Figs. 4 and 5) and were thus considered invariable for the modelling. In contrast, the Jurassic and Cretaceous strata are highly variable in thickness, and thus the magnitude of late Mesozoic burial was considered variable for the modelling (e.g. Hoth et al., 1993). Sensitivity analyses reveal that the influence of relative proportions of the Jurassic and Cretaceous thicknesses is negligible because their variation impacts the prograde thermal path only, while the thermal reset of the AFT age is mostly sensitive to the temperature at the deepest burial stage, i.e. around the onset of basin inversion. For constraining the lithological parameters, we used limestone for the Middle Triassic, siltstone for the Upper Triassic, shale and siltstone for the Jurassic, and marl for the Cretaceous sequences. The outcome of this step is a thermal path generated for the specific stratigraphic level, which was dated by
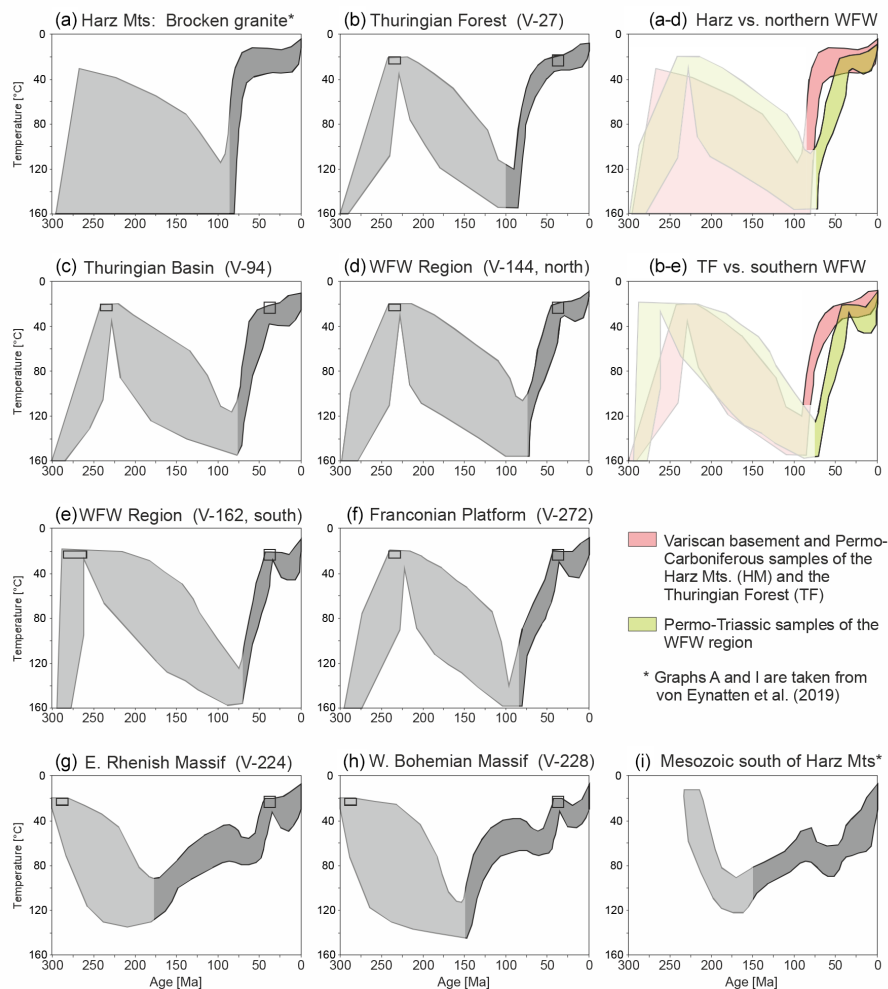
Figure 9. Time–temperature (*t T*) plots showing the envelopes of the good results of the modelling series performed on selected samples from the different regions. The modelling has been performed by HeFTy software (Ketcham, 2005) using the AFT data. Only *t T* paths classified as good fits by the programme are considered. The dark grey sections represent the well-constrained intervals of the cooling histories, while the light grey fields indicate the time–temperature regime where the modelling results carry insignificant information, as these ranges are older than the oldest fission tracks in the samples. Grey boxes indicate the time–temperature constraints when the dated samples experienced surface temperature conditions. The graphs in the upper right emphasize the contrast in the post-climax cooling paths between the exhumed basement blocks **(a, b)** and the Permo-Triassic of the WFW core region **(d, e)**.

the AFT method using the assumed burial history and heat flow.

In a second step, this thermal path was used to calculate an apatite fission-track age. The calculated age is then compared to the measured age, and according to the difference a misfit plot is constructed using the goodness of fit (GoF; see Fig. 10), which expresses the probability of failing the null hypothesis that the model and data are different (Ketcham, 2005). A detailed description of the two-step modelling procedure is given in Arató et al. (2018). Figure 10 shows the relation of the missing burial and the heat flow calculated for a sample from the Thuringian Forest and the WFW region. The negative correlation between the heat flow and the (paleo-)burial is obvious; the undulation and lenses in the plots are

artefacts related to the calculated nodes within the plotting areas. Considering heat flow values of 60–68 mW m^{-2} (see discussion below) the removed thicknesses are of the order of 3.5 to 4 km and very similar for both the TF and WFW regions. Note that assuming much higher heat flow values of 80–85 mW m^{-2} still requires removal of 2.5 to 3 km of overburden (Fig. 10).

7 Discussion

In the following we first outline the principal constraints imposed by both the new and the published thermochronological data regarding magnitudes and timing of Mesozoic to Cenozoic burial, exhumation and denudation. We then dis-
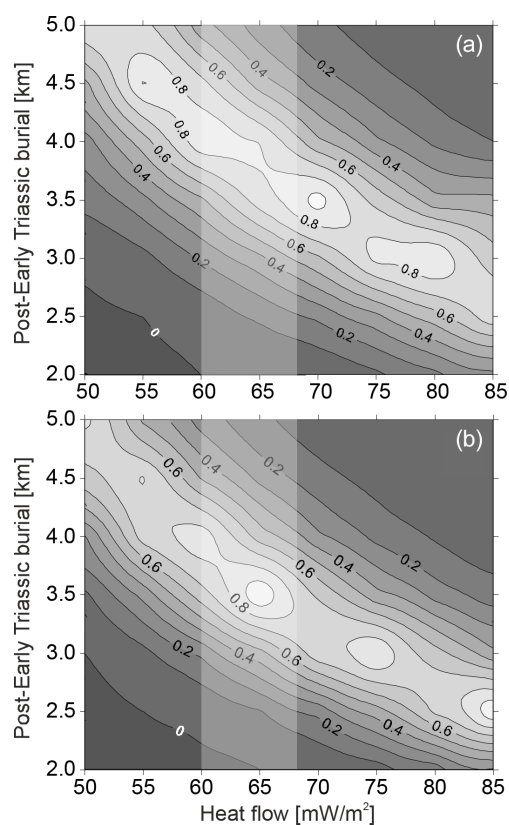
Figure 10. Modelled relations between heat flow and the thickness of the missing sequence. The plots were generated by running 56 combinations of assumed heat flow and cover sequence thicknesses using PetroMod (Schlumberger) and HeFTy (Ketcham, 2005) software. The isolines represent the goodness of fit (GoF) calculated according to the apatite fission-track ages measured on the Lower Triassic Bunter sandstone samples V-27 from the Thuringian Forest **(a)** and V-144 from the WFW region **(b)**. A high GoF value (max = 1) indicates a good match between the measured and calculated values. The burial and exhumation trends applied for the burial modelling follow the observed characteristics obtained by the thermal modelling of the Thuringian Forest and WFW samples. In case **(a)** the inflexion of the thermal history was set to 90 Ma, followed by rapid and then decreasing cooling, while in case **(b)** the inflexion is set to 75 Ma and the cooling rate is kept constant until the Eocene (see text and top right panels in Fig. 9). The light vertical band represents a most likely heat flow of 60 to 68 mW m^{-2}. The corresponding burial amounts to 3.5 to 4 km, which is actually undistinguishable for the two modelled scenarios.

cuss the validity of the range of assumed heat flow values in the light of Late Cretaceous to Paleogene volcanism. Eventually, we evaluate potential driving mechanisms for the inferred uplift and exhumation based on their magnitudes and rates. Although the discussion is focused on the main study area in central Germany, any model has to consider that the entire region which experienced Late Cretaceous to Paleogene exhumation and erosion is considerably larger, as summarized in Sect. 3.

7.1 Constraints from thermochronology and thermal modelling

Thermochronological data and modelling results in concert with sedimentological and/or stratigraphic data related to thrusted basement blocks in central Europe suggest exhumation and erosion of several kilometres of late Paleozoic to Mesozoic overburden in Late Cretaceous to Paleocene time (see Sect. 3 and Fig. 2). For the basements blocks within or adjacent to the main study area in central Germany the removed overburden amounts to at least 6 km in the case of the Harz Mountains (von Eynatten et al., 2019) and about 3–4 km in the case of the Thuringian Forest. For the latter similar values are obtained for the crystalline core (Ruhla Crystalline Complex; Thomson and Zeh, 2000) and Lower Triassic sandstones from the rim (Fig. 10a). Most of this removal occurred in Late Cretaceous time. Similar timing and magnitude have also been reported for the Flechtingen High to the north of the Harz Mountains (Fischer et al., 2012; Figs. 1 and 4).

The new thermochronological data presented for the Triassic sedimentary rocks exposed between and around the thrusted basement blocks (Fig. 7) suggest extensive exhumation and substantial erosion that are similar in magnitude to many thrusted basement blocks (i.e. 3–4 km assuming typical geothermal gradients and heat flow for continental crust; see Fig. 10 and Sect. 7.2). This regional exhumation feature holds at least for the main study area, covering about 200×300 km in central Germany and referred to here as domal uplift (Fig. 11). In contrast to the basement blocks, the areas in between, reflecting the domal uplift, are associated with significantly younger AFT ages mostly ranging from 75–55 Ma (compared to 85–70 Ma for the basement blocks, Fig. 8b). This contrast is also recorded by a later onset of cooling and exhumation in the tT paths (Fig. 9, at $\sim$ 75 Ma instead of $\sim$ 90 Ma). Overall, long tracks, narrow track length distributions and mostly tight ranges of apparent ages suggest that uplift and erosion occurred over a relatively short time interval of several million years to a few tens of million years, translating into exhumation rates of about 0.1 to 0.5 mm yr^{-1}. The 75–55 Ma age range for regional exhumation in Germany is similar to an early Cenozoic (65–55 Ma) exhumation event affecting most of the British Isles (Holford et al., 2009a, and references cited therein). Whether or not these spatially separated events reflect a common underlying process remains to be established.

Towards the margins of the study area, at the transition to the Rhenish Massif in the west and Bohemian Massif in the east, exhumation is less pronounced and extends over a longer time span (Late Jurassic to Cretaceous). Although a general trend of increasing AFT ages towards the exposed Paleozoic basement rocks is visible (Fig. 7a), the age patterns are rather heterogeneous for these two regions, most likely because the margins of the large basement massifs are structurally complex and the thickness and facies of the Mesozoic

sedimentary coverage was variable at relatively small spatial scales. The magnitudes of Late Cretaceous to Paleocene exhumation and erosion are remarkably reduced, most likely due to a combination of overall less Mesozoic burial, the lack of pronounced thrusting comparable to, e.g. the Harz Mountains, and waning uplift towards the margins of the dome. Interestingly, the tT paths for these regions (Fig. 9g and h) are rather flat at 100–75 Ma, implying relatively stable thermal conditions, which preclude both strong cooling due to exhumation and a regional thermal pulse in Late Cretaceous time. The slight increase in temperature at around 75–55 Ma appears similar to the southern rim of the Harz Mountains (Fig. 9i), where it has been interpreted as temporal burial due to storage of detritus delivered from the exhuming Harz Mountains (von Eynatten et al., 2019).

7.2 Volcanism and heat flow

Mostly Tertiary alkaline basic volcanic rocks such as basanites, nephelinites and alkali olivine basalts, along with minor occurrences of more differentiated rocks such as phonolites and trachytes, characterize the Central European Volcanic Province (Wilson and Downes, 1991; Wedepohl et al., 1994). It includes major occurrences of volcanic rocks like the Eifel, Westerwald, Vogelsberg and Rhön in central Germany (Fig. 3) and the Eger rift in the Czech Republic. Published ages vary from the middle Eocene to Quaternary; however, most occurrences are Oligocene–Miocene in age (e.g. Becker, 1993; Wedepohl et al., 1994). The Miocene Vogelsberg volcano in northern Hesse, dated between 18 and 14 Ma (Bogaard and Wörner, 2003), forms the centre of the Central European Volcanic Province with respect to both location and volume. The geochemical and isotopic characteristics of the volcanic rocks mainly suggest derivation from an upwelling asthenospheric mantle source, although some parts of the melts indicate a cooler origin in the lithosphere affected by asthenospheric melts ("veined lithospheric mantle"; Boogaard and Wörner, 2003; Jung et al., 2005). The more differentiated rocks of the Central European Volcanic Province suggest variable crustal contamination (e.g. Wörner et al., 1985; Kolb et al., 2012; Jung et al., 2013).

Although the Central European Volcanic Province is mainly a late Eocene to Miocene feature, there is widespread evidence for Late Cretaceous to Paleocene volcanic activity in the entire area. This includes zircon U–Pb ages of 70–67 Ma from trachytes and syenites from the Vogelsberg area and further occurrences to the north and south of the Odenwald (Schmitt et al., 2007; Martha et al., 2014). Similar ages (68 and 69 Ma) are reported from Ar / Ar dating of amphibole from camptonite dikes cutting the Paleozoic–Mesozoic basement of the Vogelsberg volcano (Bogaard and Wörner, 2003). Further south, along the margins of the Upper Rhine Graben, Ar / Ar dating of basic alkaline volcanic intrusions and dikes revealed Paleocene to early Eocene ages between 61 and 47 Ma (see compilation in Walter et al., 2018). Siebel

et al. (2009) reported radiometric data from zircon crystals derived from alkaline basalts of the Eger rift. Whereas the (U–Th) / He cooling ages of these zircons reflect the well-known late Oligocene eruption of the lavas, their U–Pb data suggest crystallization ages ranging from 83–51 Ma. The data reflect multiple or protracted zircon growth events or reset at different times long before eruption and suggest survival of the in zircons in a locally enriched chemical environment affected by asthenospheric upwelling processes or zircon growth in a metasomatically enriched subcontinental lithospheric mantle (Siebel et al., 2009).

The contrast between the inferred eroded thicknesses from thermochronological data for the Thuringian Forest and the significantly lower thicknesses derived from stratigraphic data for the adjacent basins led Thomson and Zeh (2000) to speculate about (i) hitherto unreported thicknesses of Jurassic to Lower Cretaceous strata (which in required thickness are only available in the Lower Saxony Basin and small confined basins like the Harz Foreland Basin, Fig. 5) and/or (ii) increased geothermal gradients. The latter, however, would have to be as high as $\sim$ 55–60 °C km^{-1} to fully account for the temperatures attained under a thin overburden. Assuming common thermal conductivity values for upper crustal rocks of 2–3 W mK^{-1} (e.g. Mielke et al., 2017), the corresponding heat flow would be about 110–180 mW m^{-2}, which is even higher than the extreme values recorded in the Pannonian Basin and most of the Basin-and-Range Province at present (Lenkey et al., 2002; Sass et al., 1994). Northeast of the study area, in the Northeast German Basin, present heat flow values range from about 70 to 90 mW m^{-2} (Norden et al., 2008). Towards the study area, these values appear to decrease to thermal gradients around 30 °C km^{-1} (Agemar et al., 2012, their Figs. 8 and 11). However, data coverage regarding the present subsurface temperature distribution is rather poor for the central German uplands region. Thermometric and thermochronological studies from the Rhenish Massif call for a "normal" and stable geothermal gradient since late Paleozoic times (Glasmacher et al., 1998; Karg et al., 2005). Further north, in the strongly inverted central and southern part of the LSB, Senglaub et al. (2005) assumed a slightly elevated gradient of about 40 °C km^{-1} during the time of maximum burial (i.e. Jurassic to Early Cretaceous).

To summarize, there is clear evidence that central Europe was affected by alkaline intraplate volcanic activity in latest Cretaceous to early Eocene time. The volumes are negligible with respect to a regional heating event throughout the crust, implying that our thermochronological data are not directly influenced by volcanic heat production. Moreover, there is no other clear evidence for large-scale and long-term increased or reduced heat flow in central Europe. Therefore, it seems justified to assume a typical gradient of $\sim$ 30 °C km^{-1} and heat flow of $\sim$ 65 mW m^{-2} for the modelling. However, the widespread occurrence of volcanic activity, although thermally insignificant, points to synchronous and large-scale processes in the asthenospheric mantle and/or across the
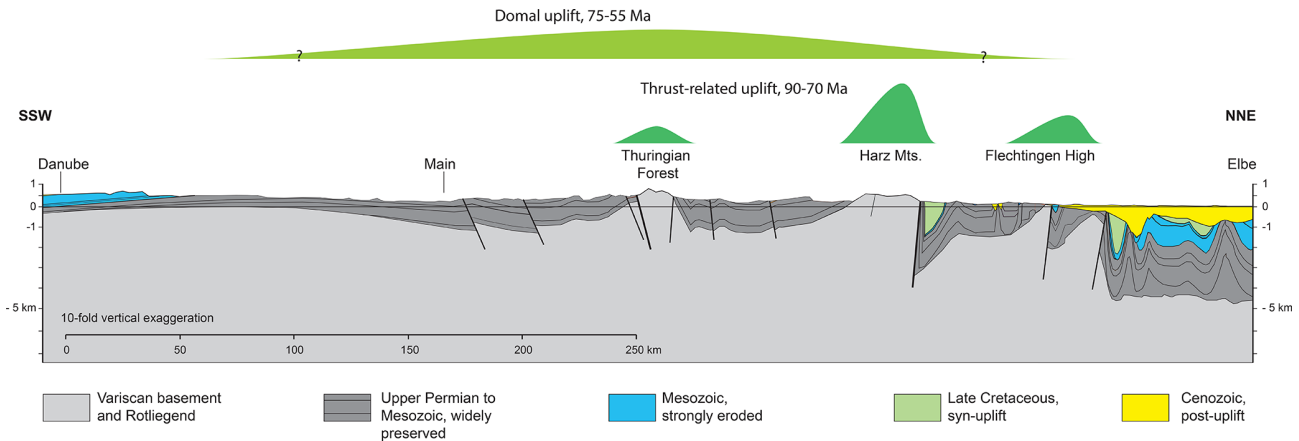
Figure 11. The two superposed uplift and exhumation processes illustrated on the cross section in Fig. 4. Thrust-related uplift confined to three discrete basement blocks is followed, possibly with some temporal overlap, by domal uplift persisting into the Paleogene. Uplift and exhumation magnitudes are not to scale.

asthenospheric–lithospheric mantle boundary that likely affected geodynamics and uplift in central Europe at that time.

7.3 Potential mechanisms for uplift, exhumation and denudation

The observable to be explained by a model for exhumation away from the thrusted basement uplifts is domal uplift of an area at least some 250–300 km across, with concomitant denudation of 3–4 km. Uplift and erosion occurred over a relatively short time interval of several million years to a few tens of million years, corresponding to exhumation rates of 0.5 to 0.1 mm yr^{-1}. Afterwards, the crust subsided slightly, as indicated by the remnants of Cenozoic marine strata, but remained significantly uplifted above its previous elevation and has not accommodated a new, thick sedimentary cover to the present. With respect to timing, this event occurred approximately 10 to 20 Myr after thrusting of the basement blocks (Figs. 8 and 9).

In general, mechanisms capable of inducing long-wavelength uplift of the continental crust can be grouped into two categories. (1) The first category is isostatic. Elevation change is caused by variations in the density and/or thickness of lithospheric materials or the asthenosphere. The crust can be thickened via tectonic shortening or addition of melt (Brodie and White, 1994; Ware and Tuner, 2002). Isostatic mechanisms involving the mantle comprise thinning of the lithospheric mantle by heating (thermal erosion) and translation of the lithosphere over more buoyant asthenosphere (Carminati et al., 2009). (2) The second category is dynamic. Uplift in this case is due to viscous stress from upwelling mantle, or it results from buckling of the crust or entire lithosphere under tangential tectonic stress.

In the following paragraphs, we derive first-order estimates of key parameters for each mechanism listed, e.g. the required magnitude of crustal shortening or lithospheric thin-

ning. We do not exclude any mechanism beforehand, but the estimated parameters suggest that some are highly unlikely. For most mechanisms it is relatively straightforward to estimate whether they could have created uplift of sufficient magnitude and rapidity. We conservatively consider 4 km of uplifted crust to be fully eroded (no topography). In the case of wholesale lithospheric uplift, the base of the lithosphere is raised by $h = 4$ km, creating room for 4 km of asthenosphere at the bottom of the column, while an equal amount of crust is eroded from the top (Fig. 12a). The pressure increase equals the load of the added asthenosphere minus the load of the eroded crust following Eq. (1):

$$\Delta p = \rho_{ast} \cdot g \cdot h - \rho_c \cdot g \cdot h \quad \text{or} \quad \Delta p = (\rho_{ast} - \rho_c) \cdot g \cdot h, \quad (1)$$

where ρ_{ast} and ρ_c are the densities of the asthenosphere and continental crust, and g is gravity acceleration. The pressure increase Δp must be compensated for by an equal but upward-directed force per area, which can be created by the addition of less dense material (for instance, rock of basaltic composition instead of mantle rock) or removal of denser material (for instance, mantle lithosphere replaced by asthenosphere). As Δp is the product of a density difference and thickness (and constant gravity acceleration), the required thickness change for any material added or lost can be calculated using Eq. (2):

$$(\rho_{ast} - \rho_c) \cdot g \cdot h = (\rho_{ast} - \rho_x) \cdot g \cdot x$$

or, eliminating g and rearranging,

$$x = h \cdot \frac{(\rho_{ast} - \rho_c)}{(\rho_{ast} - \rho_x)}, \quad (2)$$

where x and ρ_x are the thickness and density of the material added or removed. The results are listed in Table 1 and briefly discussed in the following. For the sake of simplicity, we have chosen single density values rather than ranges. The
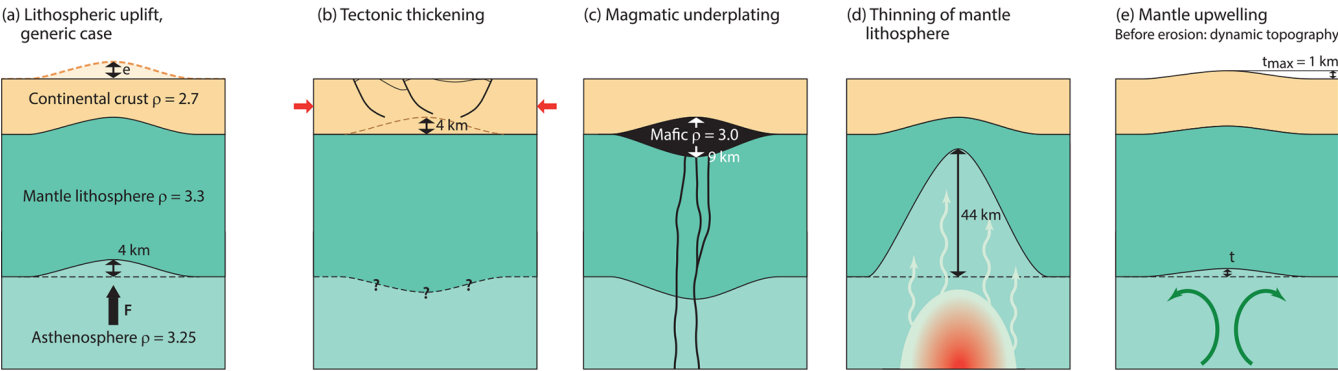
Figure 12. Scenarios for domal uplift inducing 4 km of erosion as discussed in the text. All indicated density values are in grams per cubic centimetre ($g\,cm^{-3}$). Sketches are not to scale. **(a)** Generic case of lithospheric uplift with 4 km of crust eroded and 4 km of asthenosphere added; the thickness of the lithospheric mantle is unchanged. **(b)** Crust thickened by folding and thrusting restored to original thickness by erosion. Tectonic thickening of lithospheric mantle depends on its original thickness and was not considered in our estimate. **(c)** Underplating by mafic melt. The mafic lens lifts up the Moho but does not replace continental crust. The thickness of the lithospheric mantle unchanged. **(d)** Thinning of the mantle lithosphere by thermal erosion. **(e)** Dynamic topography caused by mantle upwelling. After erosion, the configuration is similar to **(a)**, with asthenosphere replacing continental crust. In nature, **(c)**, **(d)** and **(e)** are not mutually independent. See Table 1 for a derivation of numerical values.

Table 1. Estimates of parameters for the mechanisms of uplift and exhumation discussed in the text.

Mechanism	Material x	Density	Replacing	Density	Density difference	Density difference ratio	Thickness change*	Pressure change
		($g\,cm^{-3}$)		($g\,cm^{-3}$)	($\rho_{ast}-\rho_x$)	($\rho_{ast}-\rho_c$) / ($\rho_{ast}-\rho_x$)	(km)	(MPa)
Tectonic thickening	Continental crust	2.7	Asthenosphere	3.25	0.55	1	4	22
Magmatic underplating	Basalt	3	Asthenosphere	3.25	0.25	2.2	8.8	22
Lithospheric thinning	Asthenosphere	3.25	Lithospheric mantle	3.3	−0.05	−11	−44	22
Upwelling mantle								
Surface uplift (no erosion)	Asthenosphere	3.25	Air	0	3.25	0.17	1	32.5
Erosion of crust	Asthenosphere	3.25	Continental crust	2.7	0.55	1.00	5.9	32.5

* The thickness change is calculated for 4 km of exhumation, except for the upwelling mantle case in which it is calculated from 1 km of dynamic topography.

results do not change fundamentally if densities are varied within reasonable limits.

7.3.1 Tectonic thickening of the crust

Thrusting and folding would have to thicken the crust by 4 km before erosion restores it to its original thickness (Fig. 12b). Increasing the crustal thickness in the core region from its present (and, by inference, also pre-inversion) value of 30 to 34 km requires shortening by 12 %. This is a conservative estimate because we assume that no topography is left at the end of erosion and do not consider the subsidence caused by tectonically thickened lithospheric mantle. The total shortening accommodated by folding and thrusting in Germany during Late Cretaceous inversion has been estimated at 13.5 to 15 km (Jähne et al., 2009), corresponding to an average percent shortening across the 250 km wide uplift of around 6 %. Crustal shortening could thus make a significant contribution to exhumation but not explain its full amplitude, even if the shortening accommodated by in-

dividual inversion structures may be underestimated (Eisenstadt and Withjack, 1995; Holford et al., 2009b; Bolz and Kley, 2021). The need for an additional uplift mechanism is also evidenced by the observation that structural lows such as the Thuringian Basin (syncline) did not subside but were strongly exhumed (Fig. 4). As regards the uplift rate, tectonic shortening thickens the crust at the shortening rate divided by the aspect ratio of the deforming cross-sectional area, in our case about 10 (300 km length / 30 km thickness); $1\,mm\,yr^{-1}$ of shortening would give $0.1\,mm\,yr^{-1}$ of thickening, and it would take 40 Myr to thicken the crust by 4 km. Notice, however, that this shortening rate derives from the estimated magnitude of less than 20 km shortening and does not provide an independent constraint on the capability of crustal thickening to drive exhumation.

7.3.2 Magmatic underplating

Isostatic uplift due to underplating by basaltic melts has been proposed for parts of the British Isles (e.g. Brodie and White,

1994; associated with the Iceland plume). The ca. 9 km thick column of basalt required to drive 4 km of upper crustal erosion (Fig. 12c, Table 1) is similar to the thickness of layered mafic lower crust observed in many parts of central Europe. However, this lower crust is commonly interpreted to reflect crustal re-equilibration in Permian time (e.g. Lüschen et al., 1990), and it seems unlikely that the crust before Cretaceous uplift was only 25 km thick (calculated as the pre-erosion thickness of 34 km minus 9 km of basalt). The attainable uplift rate depends on the rate of magma production. Underplating the entire area of Cretaceous uplift (ca. 70 000 km^2) by several kilometres of basaltic melt would require a magma volume typical of large igneous provinces (LIPs; e.g. Stein et al., 2018, their Fig. 8). As the production of basaltic melts can be very fast and continental flood basalts are typically erupted over only a few million years (Self et al., 2014), the emplacement rate is not limiting. However, the sparse Late Cretaceous to Paleocene volcanism makes central Europe a highly unlikely location for a LIP of that age, ruling out magmatic underplating as a driver of Late Cretaceous to Paleogene regional uplift.

7.3.3 Thinning of the lithospheric mantle

The lithospheric mantle must thin by several tens of kilometres to induce 4 km of erosion due to the small density contrast of the lithosphere and asthenosphere (Fig. 12d, Table 1). Thickness variations of the lithospheric mantle over time have been invoked to explain Mesozoic subsidence and Cenozoic uplift in central Europe (Meier et al., 2016), but the magnitude of these changes is difficult to constrain independently. Our approach of equating lithospheric thinning with replacement of constant-density lithosphere by constant-density asthenosphere is highly simplistic. The densities of the asthenosphere and subcontinental lithospheric mantle vary considerably with depth and geothermal gradient, and our chosen density contrast of 0.05 g cm^{-3} may be on the high side as an average value (Djomani et al., 2001). Duesterhoeft et al. (2012) modelled the density changes due to temperature, pressure and metamorphic reactions in a lithosphere that undergoes protracted heating from a plume impinging on its base at 1800 °C. Metamorphic density changes were responsible for 350 m out of 1400 m total uplift after 130 Myr. The effect would be smaller in our case in which the mantle temperature is presumably lower with less time available for heating. Thinning of the lithospheric mantle by upwelling asthenosphere strongly depends on the size of the uplifted area and thus the distance over which the asthenosphere spreads laterally. Semi-analytical models (Davies, 1994) suggest that an initially 120 km thick continental lithosphere can be thinned to less than 60 km within 25 Myr above a narrow plume of 70 km diameter, creating 1.5 km of non-eroded uplift, but thinning and uplift are much less efficient for an area 300 km across. However, Davies (1994) also pointed out that thinning of the lithosphere by a thermal plume is preceded

by faster dynamic uplift as the plume reaches the base of the lithosphere (see also Friedrich et al., 2018, for predicted geological effects of mantle plumes). Extremely fast removal of the continental lithosphere over only a few hundred thousand years by an impinging thermochemical plume that contains a large amount of recycled oceanic crust was modelled by Sobolev et al. (2011) but creates only about 200 m of non-eroded uplift.

7.3.4 Relative motion of the lithosphere and asthenosphere

Westward absolute motion of the European Plate over asthenosphere of lower density created at the Mid-Atlantic Ridge was proposed as a cause of Cenozoic uplift (Carminati et al., 2009). In Late Cretaceous time the mid-ocean ridge of the North Atlantic did not exist yet, and central Europe cannot have moved over depleted asthenosphere formed there. However, absolute motion could have moved central Europe over long-lived dynamic topography (see next paragraph).

7.3.5 Dynamic topography

Isostatic calculations can also be used to estimate uplift and exhumation due to mantle flow. Observational data suggest that upwelling mantle is able to sustain about 1 km of dynamic topography t (Braun et al., 2013), or 1 km of asthenosphere added to the base of the lithospheric column. If the topography is eroded while the mantle flow is maintained, the eliminated crustal load allows for additional uplift of mantle. Eventually, the load of the mantle replacing eroded crust equals that of the mantle column before erosion following Eq. (3) (Fig. 12a, e):

$$e \cdot (\rho_{ast} - \rho_c) = \rho_{ast} \cdot t \quad \text{or} \quad e = t \cdot \frac{\rho_{ast}}{(\rho_{ast} - \rho_c)} \qquad (3)$$

where e is eroded crustal thickness, t is dynamic topography, and ρ_c and ρ_{ast} are the densities of the crust and asthenosphere.

Mantle upwelling capable of sustaining 1 km of dynamic topography could thus drive some 6 km of erosion (Table 1).

The rates at which dynamic topography grows and decays depend on the mechanism assumed: topography can result from (i) a lithospheric plate moving across a stable upwelling area or swell related to long-term mantle convection (Braun et al., 2013) or (ii) a plume-like perturbation rising beneath the lithosphere. In the first case, the uplift rate depends on absolute plate velocity and the geometry of the swell. In the second case it depends on the properties of the plume. The absolute motion of Eurasia underwent major changes between 120 and 60 Ma, from a fast northwest to a slower west-directed motion at velocities decreasing from about 40 to 10 mm yr^{-1} for central Europe (Seton et al., 2012). At these velocities it would take 7.5 to 30 Myr to move a 300 km wide area onto a swell.

7.3.6 Lithospheric folding

The potential contribution of lithospheric folding to domal uplift is more difficult to assess because its amplitude strongly depends on lithosphere age and rheology as well as the magnitude and rate of shortening. Numerical modelling results indicate that folding-induced erosion can attain magnitudes way beyond the 4 km discussed here with sufficient shortening and time. On the other hand, a generic model approximately matching our case of a 300 Myr old lithosphere (thermotectonic age; Cloetingh et al., 1999) develops non-eroded topography of only 200 m amplitude at 6 % shortening (a 1500 km wide model area shortened by 90 km; Cloetingh and Burov, 2011, their Fig. 10) despite a shortening rate of 15 mm yr^{-1}, which is more than 10 to 100 times higher than Germany during Late Cretaceous time. At low shortening rates lithospheric folds take time to grow (e.g. 5–10 Myr for 1 km amplitude at 4 mm yr^{-1} for Iberia; Cloetingh et al., 2002). A stronger argument against lithospheric folding driving uplift in our case can be drawn from the large-scale structure. The area that underwent regional doming coincides with a wide syncline today (Fig. 11). Before the uplift event this syncline must have been deeper. This decrease in fold amplitude accompanying uplift cannot be the result of maintained or increased horizontal stress. It could be due to a decrease in stress if we assume that the syncline was formed or tightened by lithospheric folding (see Nielsen et al., 2005). However, since stress relaxation cannot exhume the syncline more than it was originally deepened by horizontal stress, this assumption restricts the time available for deposition of the missing overburden to the short interval of the inversion phase (90 to 75 Ma).

8 Conclusions

- A compilation of several hundred published and about 150 new thermochronological analyses (AFT and AHe) indicates generalized, kilometre-scale exhumation over substantial parts of central Europe in Late Cretaceous to Paleocene time.

- The magnitude of exhumation attains > 6 km over basement uplifts such as the Harz Mts. and 3–4 km for the other regions in central Germany.

- The spatial pattern of exhumation exhibits two types of exhumation: (i) thrust-bordered basement uplifts and (ii) superimposed regional-scale domal uplift. While thrust-related exhumation is spatially well defined, the extent of the doming area is still poorly defined.

- In detail, thrust-related uplift predates regional doming (90–70 Ma vs. 75–55 Ma) with some temporal overlap.

- Thrusting and crustal thickening associated with inversion tectonics can contribute at best half of the doming signal. An additional process or processes are required to explain the widespread exhumation.

- Thinning of the mantle lithosphere and dynamic topography, both caused by upwelling asthenosphere, are able to produce uplift of the required magnitude, wavelength and rate. The exhumed region coincides with a raised lithosphere–asthenosphere boundary at present.

- Alkaline volcanism potentially associated with mantle-induced uplift is dated at about 70–50 Ma, roughly similar to domal uplift, but its scarcity and negligible volume are puzzling.

- The apparent southern border of the Southern Permian Basin is due to exhumation. Its original depositional realm extended much further to the south in Jurassic to Early Cretaceous time.

Additional data are needed to constrain the spatial extent of domal uplift and exhumation and to decide whether it is an isolated occurrence or linked to other regions of Paleogene uplift such as the British Isles or the western and northeastern margins of the Bohemian Massif. The temporal contrast between the well-known Late Cretaceous thrusting in central Europe and the newly discovered, younger, long-wavelength domal uplift should also be investigated, verified or falsified for other regions in central Europe.

References

Agemar, T., Schellschmidt, R., and Schulz, R.: Subsurface temperature distribution in Germany, Geothermics, 44, 65–77, 2012.

Arató, R., Dunkl, I., Takács, Á., Szebényi, G., Gerdes, A., and von Eynatten, H.: Thermal evolution in the exhumed basement of a stratovolcano: case study of the Miocene Mátra Volcano, Pannonian Basin, J. Geol. Soc. London, 175, 820–835, https://doi.org/10.1144/jgs2017-117, 2018.

Augustsson, C., Voigt, T., Bernhart, K., Kreißler, M., Gaupp, R., Gärtner, A., Mofmann, M., and Linnemann, U.: Zircon size-age sorting and source-area effect: The German Triassic Buntsandstein Group, Sediment. Geol., 375, 218–231, 2018.

Bachmann, G. H., Müller, M., and Weggen, K.: Evolution of the Molasse Basin (Germany, Switzerland), Tectonophysics, 137, 77–92, 1987.

Baldschuhn, R. and Kockel, F.: Das Osning-Lineament am Südrand des Niedersachsen-Beckens, Zeitschrift der deutschen geologischen Gesellschaft, 150, 673–695, 1999.

Baldschuhn, R., Binot, F., Fleig, S., and Kockel, F.: Geotektonischer Atlas von Nordwest-Deutschland und dem deutschen Nordsee-Sektor [Tectonic Atlas of Northwest Germany and the German North Sea Sector], Geologisches Jahrbuch Reihe A, Band 153, Schweizerbart, Stuttgart, Germany, 2001.

Barbarand, J., Bour, I., Pagel, M., Quesnel, F., Delcambre, B., Dupuis, C., and Yans, J.: Post-Paleozoic evolution of the northern Ardenne Massif constrained by apatite fission-track thermochronology and geological data, Earth Sci. Bull., 189, 16, https://doi.org/10.1051/bsgf/2018015, 2018.

Becker, A.: An attempt to define a "neotectonic period" for central and northern Europe, Geol. Rundsch., 82, 67–83, 1993.

Best, G.: Floßtektonik in Norddeutschland: Erste Ergebnisse reflexionsseismischer Untersuchungen an der Salzstruktur, Zeitschrift der deutschen geologischen Gesellschaft, 147, 455–464, 1996.

Bogaard, P. J. F. and Wörner, G.: Petrogenesis of basanitic to tholeiitic volcanic rocks from the Miocene Vogelsberg, Central Germany, J. Petrol., 44, 569–602, 2003.

Boigk, H. and Schöneich, H.: The Rhinegraben: geologic history and neotectonic activity. Approaches to Taphrogenesis. Inter-Union Commission on Geodynamics, Sci. Rep., 8, 60–71, 1974.

Bolz, J. and Kley, J.: Emplacement of "exotic" Zechstein slivers along the inverted Sontra Graben (northern Hessen, Germany): clues from balanced cross-sections and geometrical forward modelling, this volume, 2021.

Botor, D., Dunkl, I, Anczkiewicz, A., and Mazur, S.: Post-Variscan thermal history of the Moravo-Silesian lower Carboniferous Culm Basin (NE Czech Republic–SW Poland), Tectonophysics, 712/713, 643–662, 2017.

Botor, D., Anczkiewicz, A. A., Dunkl, I., Golonka, J., Paszkowski, M., and Mazur, S.: Tectonothermal history of the Holy Cross Mountains (Poland) in the light of lowtemperature thermochronology, Terra Nova, 30, 270–278, https://doi.org/10.1111/ter.12336, 2018.

Braun, J., Robert, X., and Simon-Labric, T.: Eroding dynamic topography, Geophys. Res. Lett., 40, 1494–1499, 2013.

Brodie, J. and White, N.: Sedimentary basin inversion caused by igneous underplating: Northwest European continental shelf, Geology, 22, 147–150, 1994.

Büker, C.: Absenkungs-, Erosions- und Wärmeflußgeschichte des Ruhr-Beckens und des nordöstlichen Rechtsrheinischen Schiefergebirges, PhD thesis, University Bochum, Bochum, Germany, 212 pp., 1996.

Bundesanstalt für Geowissenschaften und Rohstoffe: Geologische Karte der Bundesrepublik Deutschland 1: 1,000,000, Hannover, Germany, 1993.

Bundesanstalt für Geowissenschaften und Rohstoffe: Geowissenschaftliche Karte der Bundesrepublik Deutschland 1 : 2 000 000, Hannover, Germany, 2004.

Cacace, M. and Scheck-Wenderoth, M.: Why intracontinental basins subside longer: 3-D feedback effects of lithospheric cooling and sedimentation on the exural strength of the lithosphere, J. Geophys. Res. Sol. Ea., 121, 3742–3761, https://doi.org/10.1002/2015JB012682, 2016.

Carminati, E., Cuffaro, M., and Doglioni, C.: Cenozoic uplift of Europe, Tectonics, 28, TC4016, https://doi.org/10.1029/2009TC002472, 2009.

Cloetingh, S. and Burov, E.: Lithospheric folding and sedimentary basin evolution: a review and analysis of formation mechanisms, Basin Res., 23, 257–290, 2011.

Cloetingh, S., Burov, E., Beekman, F., Andeweg, B., Andriessen, P., Garcia-Castellanos, D., De Vicente, G., and Vegas, R.: Lithospheric folding in Iberia, Tectonics, 21, 1041, https://doi.org/10.1029/2001TC901031, 2002.

Cloetingh, S. A. P. L., Burov, E., and Poliakov, A.: Lithosphere folding: Primary response to compression? (from central Asia to Paris basin), Tectonics, 18, 1064–1083, 1999.

Cooper, M. A., Williams, G. D., De Graciansky, P. C., Murphy, R. W., Needham, T., De Paor, D., Stoneley, R., Todd, S., Turner, J.P., and Ziegler, P. A.: Inversion tectonics – a discussion, in: Inversion tectonics, edited by: Williams, G. D. and Cooper, M. A.,

Geological Society Special Publications, London, UK, 335–347, 1989.

Danišík, M., Migoń, P., Kuhlemann, J., Evans, N. J., Dunkl, I., and Frisch, W.: Thermochronological constraints on the long-term erosional history of the Karkonosze Mts., Central Europe, Geomorphology, 117, 78–89, 2010.

Danišík, M., Štěpančiková, P., and Evans, N. J.: Constraining long-term denudation and faulting history in intraplate regions by multi-system thermochronology – an example of the Sudetic Marginal Fault (Bohemian Massif, Central Europe), Tectonics, 31, 1–19 https://doi.org/10.1029/2011TC003012, 2012.

Davies, G. F.: Thermomechanical erosion of the lithosphere by mantle plumes, J. Geophys. Res.-Sol. Ea., 99, 15709–15722, 1994.

Deckers, J. and van der Voet, E.: A review on the structural styles of deformation during Late Cretaceous and Paleocene tectonic phases in the southern North Sea area, J. Geodyn., 115, 1–9, 2018.

De Jager, J.: Inverted basins in the Netherlands, similarities and differences, Neth. J. Geosci., 82, 339–349, 2003.

Dielforder, A., Frasca, G., Brune, S., and Ford, M.: Formation of the Iberian-European convergent plate boundary fault and its effect on intraplate deformation in Central Europe, Geochem. Geophy. Geosy., 20, 2395–2417, 2019.

Djomani, Y. H. P., O'Reilly, S. Y., Griffin, W. L., and Morgan, P.: The density structure of subcontinental lithosphere through time, Earth Planet. Sci. Lett., 184, 605–621, 2001.

Donelick, R. A., Ketcham, R. A., and Carlson, W. D.: Variability of apatite fission-track annealing kinetics; II, Crystallographic orientation effects, Am. Mineral., 84, 1224–1234, 1999.

Donelick, R. A., O'Sullivan, P. B., and Ketcham, R. A.: Apatite fission-track analysis, Rev. Mineral. Geochem., 58, 49–94, 2005.

Doornenbal, H. and Stevenson, A.: Petroleum geological atlas of the Southern Permian Basin area: European Association of Geoscientists and Engineers (EAGE), Houten, the Netherlands, 352 pp., 2010.

Dresmann, H., Keulen, N., Timar-Geng, Z., Fügenschuh, B., Wetzel, A., and Stünitz, H.: The south-western Black Forest and the Upper Rhine Graben Main Border Fault: thermal history and hydrothermal fluid flow, Int. J. Earth Sci., 99, 285–297, 2010.

Duesterhoeft, E., Bousquet, R., Wichura, H., and Oberhänsli, R.: Anorogenic plateau formation: The importance of density changes in the lithosphere, J. Geophys. Res.-Sol. Ea., 117, B07204, https://doi.org/10.1029/2011JB009007, 2012.

Dumitru, T. A.: A new computer-automated microscope stage system for fission-track analysis, Nucl. Tracks Radiat. Meas., 21, 575–580, 1993.

Dunkl, I.: TRACKKEY: a Windows program for calculation and graphical presentation of fission track data, Comput. Geosci., 28, 3–12, 2002.

Eisenstadt, G. and Withjack, M. O.: Estimating inversion: results from clay models, Geol. Soc. London Spec. Publ., 88, 119–136, 1995.

Farley, K. A.: Helium diffusion from apatite: General behavior as illustrated by Durango fluorapatite, J. Geophys. Res., 105, 2903–2914, 2000.

Farley, K. A., Wolf, R. A., and Silver, L. T.: The effects of long alpha-stopping distance on (U-Th)/He ages, Geochim. Cosmochim. Ac., 60, 4223–4229, 1996.

Fischer, C., Dunkl, I., von Eynatten, H., Wijbrans, J. R., and Gaupp, R.: Products and timing of diagenetic processes in Upper Rotliegend sandstones from Bebertal (North German Basin, Parchim Formation, Flechtingen High, Germany), Geol. Mag., 149, 827–840, https://doi.org/10.1017/S0016756811001087, 2012.

Franke, D.: Geologie von Ostdeutschland – Ein Kompendium, available at: http://www.regionalgeologie-ost.de, last access: 18 December 2020.

Freudenberger, W. and Schwerd, K.: Erläuterungen zur Geologischen Karte von Bayern 1: 500.000, Bayerisches Geologisches Landesamt, München, Germany, 1996.

Friedrich, A. M., Bunge, H.-P., Rieger, S. M., Colli, L., Ghelichkhan, S., and Nerlich, R.: Stratigraphic framework for the plume mode of mantle convection and the analysis of interregional unconformities on geological maps, Gondwana Res., 53, 159–188, 2018.

Geluk, M.: Late Permian (Zechstein) rifting in the Netherlands; models and implications for petroleum geology, Petrol. Geosci., 5, 189–199, 1999.

Glasmacher, U., Zentilli, M., and Grist, A. M.: Apatite fission track thermochronology of Paleozoic sandstones and the Hill-intrusion, northern Linksrheinisches Schiefergebirge, Germany, in: Advances in Fission-Track Geochronology, edited by: van den Haute, P. and De Corte, F., Kluwer, Dordrech, The Netherlands, 151–172, 1998.

Glasmacher, U. A., Mann, U., and Wagner, G. A.: Thermotectonic evolution of the Barrandian, Czech Republic, as revealed by apatite fission-track analysis, Tectonophysics, 359, 381–402, 2002.

Gleadow, A. J. W.: Fission-track dating methods: what are the real alternatives?, Nuclear Tracks, 5, 3–14, 1981.

Green, P. F.: A new look at statistics in fission track dating, Nuclear Tracks, 5, 77–86, 1981.

Green, P. F.: On the thermo-tectonic evolution of Northern England: evidence from fission track analysis, Geol. Mag., 153, 493–506, 1986.

Hejl, E., Coyle, D., Lal, N., Van den Haute, P., and Wagner, G. A.: Fission-track dating of the western border of the Bohemian massif: thermochronology and tectonic implications, Geol. Rundsch., 86, 210–219, 1997.

Hejl, E., Sekyra, G., and Friedl, G.: Fission-track dating of the south-eastern Bohemian massif (Waldviertel, Austria): thermochronology and long-term erosion, Int. J. Earth Sci., 92, 677–690, 2003.

Holford, S. P., Green, P. F., Duddy, I. R., Turner, J. P., Hillis, R. R., and Stoker, M. S.: Regional intraplate exhumation episodes related to plate-boundary deformation, Geol. Soc. Am. Bull., 121, 1611–1628, 2009a.

Holford, S. P., Turner, J. P., Green, P. F., and Hillis, R. R.: Signature of cryptic sedimentary basin inversion revealed by shale compaction data in the Irish Sea, western British Isles, Tectonics, 28, TC4011, https://doi.org/10.1029/2008TC002359, 2009b.

Hoth, K., Rusbült, J., Zagora, K., Beer, H., and Hartmann, O.: Die tiefen Bohrungen im Zentralabschnitt der Mitteleuropäischen Senke: Dokumentation für den Zeitabschnitt 1962–1990, Schriftenreihe für Geowissenschaften, 2, 7–145, Verlag der Gesellschaft für Geowissenschaften, Berlin, German, 1993.

Hurford, A. J.: Zeta: the ultimate solution to fission-track analysis calibration or just an interim measure?, in: Advances in fission-

track geochronology, edited by: Van den Haute, P. and De Corte, F., Kluwer Academic Publishers, Dordrecht, the Netherlands, 19–32, 1998.

Hurford, A. J. and Green, P. F.: The zeta age calibration of fission-track dating, Chem. Geol. Isot. Geosci., 41, 285–312, 1983.

Jacobs, J. and Breitkreuz, C.: Zircon and apatite fission-track thermochronology of Late Carboniferous volcanic rocks of the NE German Basin, Int. J. Earth Sci., 92, 165–172, 2003.

Jähne, F., Kley, J., Hoffmann, V. E., von Eynatten, H., and Dunkl, I.: Timing and Kinematics of Cretaceous to Paleogene inversion at the SE margin of the Central European Basin System: Part 1, Kinematics, EGU General Assembly, Vienna, Austria, 19–24 April 2009, EGU2009-8176, 2009.

Jung, S., Pfänder, J. A., Brügmann, G., and Stracke, A.: Sources of primitive alkaline volcanic rocks from the central European Volcanic province (Rhön, Germany) inferred from Hf, Pb and Os isotopes, Contrib. Mineral. Petr., 150, 546–559, 2005.

Jung, S., Mezger, K., Hauff, F., Pack, A., and Hoernes, S.: Petrogenesis of rift-related tephrites, phonolites and trachytes (Central European Volcanic Province, Rhön, FRG): Constraints from Sr, Nd, Pb and O isotopes, Chem. Geol., 354, 203–215, 2013.

Kämmlein, M., Bauer, W., and Stollhofen, H.: The Franconian Basin thermal anomaly, SE Germany revisited: New thermal conductivity and uniformly corrected temperature data, J. Appl. Reg. Geol., 171, 21–44, 2020.

Karg, H., Carter, A., Brix, M. R., and Littke, R.: Late- and post-Variscan cooling and exhumation history of the northern Rhenish massif and the southern Ruhr Basin: new constraints from fission-track analysis, Int. J. Earth Sci., 94, 180–192, 2005.

Ketcham, R. A.: Forward and inverse modeling of low-temperature thermochronometry data, Rev. Mineral. Geochem., 58, 275–314, 2005.

Ketcham, R. A., Carter, A., Donelick, R. A., Barbarand, J., and Hurford, A. J.: Improved modeling of fission-track annealing in apatite, Am. Mineral., 92, 799–810, https://doi.org/10.2138/am.2007.2281, 2007.

Kley, J.: Timing and spatial patterns of Cretaceous and Cenozoic inversion in the Southern Permian Basin, in: Mesozoic Resource Potential of the Southern Permian Basin, edited by: Kilhams, B., Kukla, P. A., Mazur, S., McKie, T., Munlieff, H. F., and van Ojik, K., Geological Society, London, Special Publications, 469, 19–31, https://doi.org/10.1144/SP469.12, 2018.

Kley, J. and Voigt, T.: Late Cretaceous intraplate thrusting in central Europe: effect of Africa-Iberia-Europe convergence, not Alpine collision, Geology, 36, 839–842, 2008.

Kley, J., Franzke, H. J., Jähne, F., Krawczyk, C., Lohr, T., Reicherter, K., Scheck-Wenderoth, M., Sippel, J., Tanner, D., and van Gent, H.: The SPP Structural Geology Group: Strain and Stress (Chapter 3.3), in: Dynamics of Complex Intercontinental Basins – the Central European Basin System, edited by: Littke, R., Bayer, U., Gajewski, D., and Nelskamp, S., Springer-Verlag, Berlin and Heidelberg, Germany, 97–124, 2008.

Kockel, F.: Inversion structures in central Europe – Expressions and reasons, an open discussion, Neth. J. Geosci., 82, 367–382, 2003.

Kolb, M., Paulick, H., Kirchenbaur, M., and Münker, C.: Petrogenesis of mafic to felsic lavas from the Oligocene Siebengebirge Volcanic Field (Germany): implications for the origin of intra-continental volcanism in Central Europe, J. Petrol., 53, 2349–2379, 2012.

Kroner, U., Mansy, J. L., Mazur, S., Aleksandrowski, P., Hann, H. P., Huckriede, H., Lacquement, F., Lamarche, J., Ledru, P., Pharaoh, T. C., Zedler, H., Zeh, A., and Zulauf, G.: The Geology of Central Europe, Vol. 1: Precambrian and Palaeozoic, in: Variscan Tectonics, edited by: McCann, T., Geological Society, London, UK, 599–664, 2008.

Krzywiec, P.: Mid-Polish Trough inversion – seismic examples, main mechanisms and its relationship to the Alpine-Carpathian collision, Stephan Mueller Special Publication Series, 1, 151–165, https://doi.org/10.5194/smsps-1-151-2002, 2002.

Krzywiec, P.: Structural inversion of the Pomeranian and Kuiavian segments of the Mid-Polish Trough – lateral variations in timing and structural style, Geol. Q., 50, 151–168, 2006.

Krzywiec, P. and Stachowska, A.: Late Cretaceous inversion of the NW segment of the Mid-Polish Trough – how marginal troughs were formed, and does it matter at all?, Zeitschrift der deutschen geologischen Gesellschaft, 167, 107–119, 2016.

Krzywiec, P., Gutowski, J., Walaszczyk Wróbel, G., and Wybraniek, S.: Tectonostratigraphic model of the Late Creta ceous in ver sion along the Nowe Miasto–Zawichost Fault Zone, SE Mid-Polish Trough, Geol. Q., 53, 27–48, 2009.

Lange, J.-M., Tonk, C., and Wagner, G. A.: Apatite fission track data for the Postvariscan thermotectonic evolution of the Saxon basement – first results, Zeitschrift der deutschen geologischen Gesellschaft, 159, 123–132, 2008.

Lenkey, L., Dövényi, P., Horváth, F., and Cloetingh, S. A. P. L.: Geothermics of the Pannonian basin and its bearing on the neo-tectonics, Stephan Mueller Special Publication Series, 3, 29–40, https://doi.org/10.5194/smsps-3-29-2002, 2002.

Link, K.: Die thermo-tektonische Entwicklung des Oberrheingraben-Gebietes seit der Kreide, PhD Thesis, Albert-Ludwigs-Universität, Freiburg, Germany, 373 pp., 2009.

Linnemann, U., D'Lemos, R., Drost, K., Jeffries, T., Gerdes, A., Romer, R. L., Samson, S. D., and Strachan, R. A.: Cadomian Tectonics, in: The Geology of Central Europe, Vol. 1: Precambrian and Palaeozoic, edited by: McCann, T., Geological Society, London, UK, 103–154, 2008.

Littke, R., Bayer, U., Gajewski, D., and Nelskamp, S.: Dynamics of complex intracontinental basins: the central European basin system, Springer, Berlin, Germany, 2008.

Lorenz, V. and Nicholls, I. A.: The Permocarboniferous basin and range province of Europe. An application of plate tectonics, in: The Continental Permian in Central, West, and South Europe, Springer, Dordrecht, The Netherlands, 1976.

Lotze, F.: 100 Jahre Forschung in der saxonischen Tektonik, Zeitschrift der deutschen geologischen Gesellschaft, 100, 321–337, 1948.

Lüschen, E., Nolte, B., and Fuchs, K.: Shear-wave evidence for an anisotropic lower crust beneath the Black Forest, southwest Germany, Tectonophysics, 173, 483–493, 1990.

Malz, A., Madritsch, H., and Kley, J.: Improving 2D seismic interpretation in challenging settings by integration of restoration techniques: A case study from the Jura fold-and-thrust belt (Switzerland), Interpretation, 3, 37–58, 2015.

Malz, A., Nachtweide, C., Emmerlich, S., and Schimpf, L.: Mesozoic intraplate deformation in the southern part of the Central European Basin-Results from large-scale 3D modelling, Tectonophysics, 776, 228315, https://doi.org/10.1016/j.tecto.2019.228315, 2020.

Martha, S. O., Zulauf, G., Dörr, W., Nesbor, H.-D., Petschick, R., Prinz-Grimm, P., and Gerdes, A.: The Saxothuringian-Rhenohercynian boundary underneath the Vogelsberg volcanic field: evidence from basement xenoliths and U-Pb zircon data of trachyte, Zeitschrift der deutschen geologischen Gesellschaft, 165, 373–394, 2014.

Meier, T., Soomro, R. A., Viereck, L., Lebedev, S., Behrmann, J. H., Weidle, C., Cristiano, L., and Hanemann, R.: Mesozoic and Cenozoic evolution of the Central European lithosphere, Tectonophysics, 692, 58–73, 2016.

Meyer, H., Hetzel, R., Fügenschuh, B., and Strauss, H.: Determining the growth rate of topographic relief using in situ-produced ^{10}Be: a case study in the Black Forest, Germany, Earth Planet. Sci. Lett., 290, 391–402, 2010.

Mielke, P., Bär, K., and Sass, I.: Determining the relationship of thermal conductivity and compressional wave velocity of common rock types as a basis for reservoir characterization, J. Appl. Geophys., 140, 135–144, 2017.

Migoń, P. and Danišík, M.: Erosional history of the Karkonosze Granite Massif – Constraints from adjacent sedimentary basins and thermochronology, Geol. Q., 56, 441–456, 2012.

Mohr, M., Kukla, P. A., Urai, J. L., and Bresser, G.: Multiphase salt tectonic evolution in NW Germany: seismic interpretation and retro-deformation, Int. J. Earth Sci., 94, 917–940, 2005.

Nielsen, S. B., Thomsen, E., Hansen, D. L., and Clausen, O. R.: Plate-wide stress relaxation explains European Palaeocene basin inversions, Nature, 435, 195–198, 2005.

Norden, B., Förster, A., and Balling, N.: Heat Flow and lithospheric thermal regime in the Northeast German Basin, Tectonophysics, 460, 215–229, 2008.

Oncken, O.: Transformation of a magmatic arc and an orogenic root during oblique collision and it's consequences for the evolution of the European Variscides (Mid-German Crystalline Rise), Geol. Rundsch., 86, 2–20, 1997.

Sass, J. H., Lachenbruch, A. H., Galanis Jr., S. P., Morgan, P., Priest, S. S., Moses Jr., T. H., and Munroe, R. J.: Thermal regime of the southern Basin and Range Province: 1. Heat flow data from Arizona and the Mojave Desert of California and Nevada, J. Geophys. Res.-Sol. Ea., 99, 22093–22119, 1994.

Schmitt, A. K., Marks, M. A., Nesbor, H. D., and Markl, G.: The onset and origin of differentiated Rhine Graben volcanism based on U-Pb ages and oxygen isotopic composition of zircon, Eur. J. Mineral., 19, 849–857, 2007.

Schönig, J., von Eynatten, H., Meinhold, G., Lünsdorf, N. K., Willner, A. P., and Schulz, B.: Deep subduction of felsic rocks hosting UHP lenses in the central Saxonian Erzgebirge: Implications for UHP terrane exhumation, Gondwana Res., 87, 320–329, 2020.

Seidel, G.: Geologie von Thüringen, Schweizerbart, Stuttgart, Germany, 2003.

Self, S., Schmidt, A., and Mather, T. A.: Emplacement characteristics, time scales, and volcanic gas release rates of continental flood basalt eruptions on Earth, Geol. Soc. Am. Spec. Pap., 505, https://doi.org/10.1130/2014.2505(16), 2014.

Senglaub, Y., Littke, R., and Brix, M. R.: Numerical modelling of burial and temperature history as an approach for an alternative interpretation of the Bramsche anomaly, Lower Saxony Basin, Int. J. Earth Sci., 95, 204–224, 2005.

Seton, M., Müller, R. D., Zahirovic, S., Gaina, C., Torsvik, T., Shephard, G., Talsma, A., Gurnis, M., Turner, M., Maus, S., and Chandler, M.: Global continental and ocean basin reconstructions since 200Ma, Earth-Sci. Rev., 113, 212–270, 2012.

Siebel, W., Schmitt, A. K., Danišík, M., Chen, F., Meier, S., Weiss, S., and Eroglu, S.: Prolonged mantle residence of zircons xenocrysts from the western Eger rift, Nat. Geosci., 2, 886–890, https://doi.org/10.1038/NGEO695, 2009.

Sissingh, W.: Syn-kinematic palaeogeographic evolution of the West European Platform: correlation with Alpine plate collision and foreland deformation, Neth. J. Geosci., 85, 131–180, 2006.

Sobczyk, A., Danišík, M., Aleksandrowski, P., and Anczkiewicz, A.: Post-Variscan cooling history in the central Western Sudetes (NE Bohemian Massif) and its implications for topographic evolution: Insights from apatite fission-track and zircon (U-Th)/He thermochronology, Tectonophysics, 649, 47–57, 2015.

Sobczyk, A., Sobel, E. R., and Georgieva, V.: Meso-Cenozoic cooling and exhumation history of the Orlica-Śnieżnik Dome (Sudetes, NE Bohemian Massif, Central Europe): Insights from apatite fission-track thermochronometry, Terra Nova, 32, 122–133, https://doi.org/10.1111/ter.12449, 2020.

Sobolev, S. V., Sobolev, A. V., Kuzmin, D. V., Krivolutskaya, N. A., Petrunin, A. G., Arndt, N. T., Radko, V. A., and Vasiliev, Y. R.: Linking mantle plumes, large igneous provinces and environmental catastrophes, Nature, 477, 312–316, 2011.

Stackebrandt, W. and Franzke, H. J.: Alpidic reactivation of the Variscan consolidated lithosphere – the activity of some fracture zones in Central Europe, Z. Geol. Wissenschaft., 17, 699–712, 1989.

Stein, S., Stein, C. A., Elling, R., Kley, J., Keller, G. R., Wysession, M., Rooney, T., Frederiksen, A., and Moucha, R.: Insights from North America's failed Midcontinent Rift into the evolution of continental rifts and passive continental margins, Tectonophysics, 744, 403–421, 2018.

Stollhofen, H., Bachmann, G. H., Barnasch, J., Bayer, U., Beutler, G., Franz, M., Kästner, M., Legeler, B., Mutterlose, J., and Radies, D.: Upper Rotliegend to Early Cretaceous basin development, in: Dynamics of Complex Intracontinental Basins. The Central European Basin System, edited by: Littke, R., Bayer, U., Gajewski, D., and Nelskamp, S., Springer-Verlag, Berlin and Heidelberg, Germany, 181–210, 2008.

Suchý, V., Filip, J., Sýkorová, I., Pesek, J., and Korínková, D.: Palaeo-thermal and coalification history of Permo-Carboniferous sedimentary basins of Central and Western Bohemia, Czech Republic: first insights from apatite fission track analysis and vitrinite reflectance modelling, B. Geosci., 94, 201–219, 2019.

Thomson, S. N. and Zeh, A.: Fission-track thermochronology of the Ruhla Crystalline Complex: new constraints on the post-Variscan thermal evolution of the NW Saxo-Bohemian Massif, Tectonophysics, 324, 17–35, 2000.

Timar-Geng, Z., Fügenschuh, B., Wetzel, A., and Dresmann, H.: Low-temperature thermochronology of the flanks of the southern Upper Rhine Graben, Int. J. Earth Sci., 95, 685–702, 2006.

Vamvaka, A., Siebel, W., Chen, F., and Rohrmuller, J.: Apatite fission-track dating and low-temperature history of the Bavarian Forest (southern Bohemian Massif), Int. J. Earth Sci., 103, 103–119, 2014.

Ventura, B. and Lisker, F.: Long-term landscape evolution of the northeastern margin of the Bohemian Massif: apatite fission-track data from the Erzgebirge (Germany), Int. J. Earth Sci., 92, 691–700, 2003.

Ventura, B., Lisker, F., and Kopp, J.: Thermal and denudation history of the Lusatian Block (NE Bohemian Massif, Germany) as indicated by apatite fission-track data, Geol. Soc. Spec. Publ., 324, 1–12, 2009.

Voigt, E.: Über Randtröge vor Schollenrändern und ihre Bedeutung im Gebiet der Mitteleuropäischen Senke und angrenzender Gebiete, Z. Dtsch. Geol. Ges., 114, 378–418, 1963.

Voigt, T., von Eynatten, H., and Franzke, H. J.: Late Cretaceous unconformities in the Subhercynian Cretaceous Basin (Germany), Acta Geol. Pol., 54, 765–765, 2004.

Voigt, T., Wiese, F., von Eynatten, H., Franzke, H.-J., and Gaupp, R.: Facies evolution of syntectonic Upper Cretaceous Deposits in the Subhercynian Cretaceous Basin and adjoining areas (Germany), Zeitschrift der deutschen geologischen Gesellschaft, 157, 203–244, 2006.

Voigt, T., von Eynatten, H., and Kley, J.: Kommentar zu Nördliche Harzrandstorung: Diskussionsbeitrage zu Tiefenstruktur, Zeitlichkeit und Kinematik von Volker Wrede (ZDGG 159, 293–316), Zeitschrift der deutschen gesellschaft für Geowissenschaften, 160, 93–99, 2009.

Voigt, T., Kley, J., and Voigt, S.: Dawn and Dusk of Late Cretaceous Basin Inversion in Central Europe, this volume, 2021.

von Eynatten, H., Voigt, T., Meier, A., Franzke, H.-J., and Gaupp, R.: Provenance of the clastic Cretaceous Subhercynian Basin fill: constraints to exhumation of the Harz Mountains and the timing of inversion tectonics in the Central European Basin, Int. J. Earth Sci., 97, 1315–1330, 2008.

von Eynatten, H., Dunkl, I., Brix, M., Hoffmann, V.-E., Raab, M., Thomson, S. N., and Kohn, B.: Late Cretaceous exhumation and uplift of the Harz Mountains, Germany: a multi-method thermochronological approach, Int. J. Earth Sci., 108, 2097–2111, https://doi.org/10.1007/s00531-019-01751-5, 2019.

Wagner, G. A.: Fission track dating of apatites, Earth Planet. Sci. Lett., 4, 411–415, 1968.

Walter, B. F., Gerdes, A., Kleinhanns, I. C., Dunkl, I., von Eynatten, H., Kreissl, S., and Markl, G.: The connection between hydrothermal fluids, mineralization, tectonics and magmatism in a continental rift setting: Fluorite Sm-Nd and hematite and carbonates U-Pb geochronology from the Rhinegraben in SW Germany, Geochim. Cosmochim. Ac., 240, 11–42, 2018.

Ware, P. D. and Turner, J. P.: Sonic velocity analysis of the Tertiary denudation of the Irish Sea basin, Geol. Soc. Spec. Publ., 196, 355–370, 2002.

Warsitzka, M., Jähne-Klingberg, F., Kley, J., and Kukowski, N.: The timing of salt structure growth in the Southern Permian Basin (Central Europe) and implications for basin dynamics, Basin Res., 31, 337–360, 2019.

Wedepohl, K. H., Gohn, E., and Hartmann, G.: Cenozoic alkali basaltic magmas of western Germany and their products of differentiation, Contr. Min. Petrol., 115, 253–278, 1994.

Wetzel, A., Allenbach, R., and Allia, V.: Reactivated basement structures affecting the sedimentary facies in a tectonically "quiescent" epicontinental basin: an example from NW Switzerland, Sediment. Geol., 157, 153–172, 2003.

Wilson, M. and Downes, H.: Tertiary-Quaternary extension-related alkaline magmatism in western and central Europe, J. Petrol., 32, 811–849, 1991.

Wolff, R., Dunkl, I., Lange, J.-M., Tonk, C., Voigt, T., and von Eynatten, H.: Superposition of burial and hydrothermal events: post-Variscan thermal evolution of the Erzgebirge, Germany, Terra Nova, 27, 292–299, 2015.

Wörner, G., Staudigel, H., and Zindler, A.: Isotopic constraints on open system evolution of the Laacher See magma chamber (Eifel, West Germany), Earth Planet. Sci. Lett., 75, 37–49, 1985.

Xu, C., Mansy, J. L., van den Haute, P., Guillot, F., Zhou, Z., Chen, J., and de Grave, J.: Late- and post-Variscan evolution of the Ardennes in France and Belgium: constraints from apatite fission-track data, Geol. Soc. Spec. Publ., 324, 167–179, 2009.

Ziegler, P. A.: Late Cretaceous and Cenozoic intra-plate compressional deformations in the Alpine foreland – a geodynamic model, Tectonophysics, 137, 389–420, 1987.

Ziegler, P. A.: Geological Atlas of Western and Central Europe, Shell Internationale Petroleum Mij, BV and Geological Society of London, 2nd Edn., London, UK, 239 pp., 1990.

Ziegler, P. A., Cloetingh, S., and van Wees, J. D.: Dynamics of intra-plate compressional deformation: the Alpine foreland and other examples, Tectonophysics, 252, 7–59, 1995.